



UNIVERSITÀ
DI TRENTO

Dipartimento di Ingegneria e Scienza dell'Informazione

Corso di Laurea in
Ingegneria Informatica, delle Comunicazioni ed Elettronica

ELABORATO FINALE

STATIC AND RECONFIGURABLE
METASURFACES

Supervisore

.....

Laureando

Tairovski Denis

Anno accademico 21/22

Contents

Sommario	1
1 Introduction	2
1.1 What are Meta-Surfaces?	2
1.2 Passive Meta-Surfaces	3
1.3 Active Meta-Surfaces	3
2 State-of-Art Analysis	3
2.1 Holographic Smart EM Skins for Advanced Beam Power Shaping in Next Generation Wireless Environments [8]	4
2.1.1 Motivation and Principles	4
2.1.2 Mathematical Formulation and Design Formulas	5
2.1.3 Synthesis Procedure	8
2.1.4 Numerical Results	10
3 Planning EM	16
3.1 Introduction	16
3.2 Scenario	16
3.2.1 Parameters	16
3.2.2 Power and Threshold	17
3.2.3 Region of Interest	17
3.2.4 Smart Skins Choice	18
3.2.5 Enhancement Region of Interest 1	19
3.2.6 Enhancement Region of Interest 2	22
3.2.7 Enhancement Region of Interest 3	25
4 Conclusions	27
4.1 State-of-Art Conclusions	27
4.2 Planning EM Conclusions	28
4.3 Final conclusions	29
Bibliografia	30

Summary

This discourse aims to describe and analyze the work behind Meta-Surfaces. A mathematical description of various meta-surfaces is provided, emphasizing the need to create a Meta-Surface adapted to the environment where it is going to be placed. After that, a practical description is provided, having

an existing scenario to be improved. To achieve that, various Meta-Surfaces are going to be employed, having different scenarios discussed. To obtain the described goal, various tools are used, such as the Feko Winprop Suite, the Ansys HFSS Suite and GNUMPlot scripts provided. As for the conclusions, the goal has been greatly achieved, with an extended discussion for every step.

Chapter 1

Introduction

During these last 20 years, the technology had a massive improvement. Cellular communication first started with smart-phones, which were an absolute revolution in terms of portable communication, User-Interface, portability, etc. And, along with the smart-phone, new standard of communication had to be made in order to meet the user needs in terms of Data-Transfer, Reliability and Quality of Service. After the massive success of 1G, deployed in 1979, and 2G, in 1991, 3G, 2011, was a huge advancement in terms of download speed. Users had the opportunity to surf the net and stream music, which was impossible with 2G, even though it had the same capabilities but not the same speed. It wasn't until 2007, the year the first iPhone came out, that the demand for faster and more reliable network capabilities put ISPs under pressure. Not long after that, in 2009, 4G was finally deployed and, needless to say, since it's even used nowadays, in 2022, it was, and it still is, a huge success. Speed, Reliability, Quality. All those factor had to be taken in account for explaining the huge impact this standard of communication had brought into the telecommunication world. For over 10 years, 4G is still the most common standard used in smart-phones. The only improvement it needs is faster speed. Since the technology is evolving by the second, faster data transfer is an irremovable requirement. That's why 5G is the most valid option. With 20 times the average speed of 4G, and an incredibly low latency, it should be everyone is waiting for. But it comes with a huge downside: it's frequency. Since it works with much higher frequencies, between 30 GHz and 300 GHz, its wavelength is much smaller, and since it's been considered a urban environment, it's really difficult to have Reliability and Quality of Service compared to those of 4G. That's why the developing and deploying of Meta-Surfaces is needed. Let's explain what Meta-Surfaces actually are.

1.1 What are Meta-Surfaces?

Meta-Surfaces(MS) is a device that allow to control the wireless propagation environment via an array of passive or reconfigurable reflecting elements. With the continuous improving of the urban environment, 4G and 5G antennas have a much harder job. ISPs and antennas manufacturers tried some ways to overcome the problem, like transmitting more power, using new frequency bands or installing more Base-Station (BS). But all those "apparent solutions" are not fitted for the job, since the need for less power consumption and budget-friendly solution is needed. A possible countermeasure is to use the problem to find a solution. Using the environment to improve the signal emitted from the BS is what MSs are for. MSs are simply tiles of reflective material that helps with the coverage of the signal emitted from a BS. Since it is going to be used a lot in urban environment, the need to be invisible or not obstructive to the eye is needed. It could be a panel or a paint applicable on the facade of a building. And, if more MSs are combined in a urban environment, what could be achieved is a Smart-Electromagnetic-Environment (SEME or SEE). MSs are split in two categories: Passive or Re-configurable. Passive MSs, also known as Electromagnetic Skins (EMS) or Intelligent Reflective Surfaces (IRS), are essentially pieces of reflective material that are placed on the facades of buildings. Re-configurable MSs, also known as Re-Configurable Intelligent Reflective Surfaces (RIRS),

are reflective surfaces with the ability to actively adjust the reflective angle for better coverage. Let's examine both of these surfaces.

1.2 Passive Meta-Surfaces

As previously said, Passive Meta-Surfaces (PMS) are, essentially, reflective Surfaces placed, usually, on facades of building to improve coverage of the BS. They are composed by capacitive elements located ad sub-wavelength distance from a metallic plane. Each cell is loaded with active components in order to control the phase and the amplitude of the reflection coefficient. In these last years, this technology has emerged as a promising solution to improve wireless coverage, thanks to the fact that the amplitude and/or phase shift are tunable at each of its large number of reflecting elements. But the most crucial point is the ability to operate without power amplifiers. Each unit cell can be tuned such that signals bouncing off a RIS are combined constructively to increase signal in the position of the intended receiver or destructively to avoid leaking signals to undesired receivers. Another focus point it's its mechanical design: since it's light weight, it can easily be coated with the environment. But, even though it's really easy to configure and install, it has a big downside: passive-IRS aided systems may be constrained by its high path-loss. Many solutions have been suggested, such as installing a large number of passive reflecting elements, deploying the passive-IRS near the BS. But those solutions have been proved inadequate for the purpose. Even though IRSs can be equipped with radio-frequency switches, this solution it's economically impractical. That's why, in some cases, active-IRSs are needed.

1.3 Active Meta-Surfaces

As explained before, passive Meta-Surfaces, are inconvenient in some cases. Since the environment could be filled with building or have a lot of open areas, there are some cases when moving the Meta-Surface is physically impossible, and its passive power amplification and phase shift are not enough to improve the quality of the signal. That's why, in some cases, the deployment of active-IRSs is necessary. IPSs have to consider the hardware and energy cost, which in most cases is a massive downside.

Chapter 2

State-of-Art Analysis

This Section is focused on the detailed analysis (HL-SoA) of the design methodology proposed in [8].

ID	Year	Title	Journal	Authors
Oliveri.2021	2021	Holographic Smart EM Skins for Advanced Beam Power Shaping in Next Generation Wireless Environments	IEEE J. Multi-scale Multiphys. Comput. Tech	G. Oliveri, P. Rocca, M. Salucci and A. Massa

2.1 Holographic Smart EM Skins for Advanced Beam Power Shaping in Next Generation Wireless Environments [8]

2.1.1 Motivation and Principles

As the technology moves forward, a much larger quantity of data needs to travel. Nowadays, everything can be done using a mobile device and in order to secure a stable connection, the wireless cellular system need to fulfill a various number of requirements, such as transfer speed, flexibility, coverage, reliability and quality of service. Since the urban environments is in a continuous state of change, the Base Station is incapable to rely on itself. Since the upgrading of the upgrading of the technology behind the Base Stations or the cellular device has its limits, it's fundamental to use the urban environment as efficiently as possible. Every urban environment as much wider and taller building that interrupts the Line-Of-Sight between Base Station and User. That's the main point of creating a Smart Electromagnetic Environment (SEE). Thanks to a SEE, the environment acquires the ability to adapt itself to help fulfilling all those previous citated requirements and, subsequently, the scenario becomes a controllable part of a wireless system . In order to adapt the environment, we use thin meta-surfaces operating as Smart Electromagnetic (EM) Skins. Thanks to this technology, the manipulation of the reflected/transmitted wavefront, at a meta-atomic level, to overcome Snell's Law, is possible. Snell's Law states that, in very simple terms, "input and output angle are the same". This constraint implies a large set of unconventional phenomena, such as anomalous reflections or perfect absorption. On the other hand, dynamically adjustable artificial materials operating as Reconfigurable Intelligent Surfaces (RIS) give the control of the reflected wave properties in realtime, implying non-negligible implementation complexity, costs and power consumption. On the contrary, static passive smart EM skins (SPSSs) imply no running costs after installation and they potentially have advanced beamforming and contoured footprint radiation capabilities when featuring a holographic layout, therefore enabling to increase the coverage and reduce blind spot regions in urban wireless communications. The negative side of SPSSs are its degrees-of-freedom (DoFs); since the DoFs are severely constrained in terms of the final layout complexity, its design is very challenging. One characteristic that SPSSs need to have is its size: the size of a SPSSs need to be large enough to reflect an adequate quantity of power to the coverage area but it needs to respect some size limitations in order to not be excessively big. Furthermore, another DoFs that could be considered is the surface orientation; even though its control is limited, its usability to enhance the performance of the SPSSs, respecting the incident direction of the illuminating beam, is necessary. The objective of this paper is to give some indications on the feasibility of simple and inexpensive holographic SPSSs suitable for advanced wave manipulation and beamforming. To achieve this, the need to formulate a complex multiscale EM design problem within the Generalized Sheet Transition Condition (GSTC) theoretical framework is needed. A phase-only inverse source (IS) is adopted to generalize concepts, such as the non-uniqueness of the radiation operator due to the existence of non-radiating (NR) currents for reflect-array engineering to the synthesis of a holographic meta-surface working in the SEE scenario. The footprint coverage capabilities of the smart EM skin are successively optimized by combining:

- a local search approach, based on Iterative Projection Technique (IPT): aims at deducing the reference/ideal surface currents affording the user-defined footprint pattern;
- a customized version of the System-by-Design (SbD) paradigm: sets the descriptors of the SPSSs for matching these reference currents

Such methodological choices in the implementation of a synthesis method for SPSSs are driven by:

- accuracy of GSTC theory in accounting of the complex EM response of smart skins in the SEE environment;
- effectiveness of the SbD in handling complex multi-scale design problems;
- intrinsic advantages of exploiting an IS formulation when determining surface currents;

Consequently, the main innovative contributions of this work lie in:

- customization of the SbD paradigm within the GSTC framework;
- combination of the SbD-based technique and of an IPT-based source synthesis process to afford complex pattern footprints with simple and inexpensive SPSS layouts;
- numerical assessment of the effectiveness of the proposed approach as well as of the feasibility of holographic SPSSs able to generate complex footprints.

To asses correctly the stated problem, the following auxiliary papers

ID	Year	Title	Journal	Authors
Yang.2021	2021	Surface Electromagnetics With Applications in Antenna, Microwave and Optical Engineering	Cambridge Univ. Press	F. Yang and Y. Rahmat-Sanni
Salucci.2018	2018	Synthesis of shaped beam reflectarrays with constrained geometry by exploiting non-radiating surface currents	IEEE Trans. Antennas Propag	M. Salucci et al.

will be used, since they contain a needed case study. It's worth pointing out that the [8] has more references, but for the sake of the formulation, only these are needed, since they contain important experiments that cannot be vastly explained in this discussion.

2.1.2 Mathematical Formulation and Design Formulas

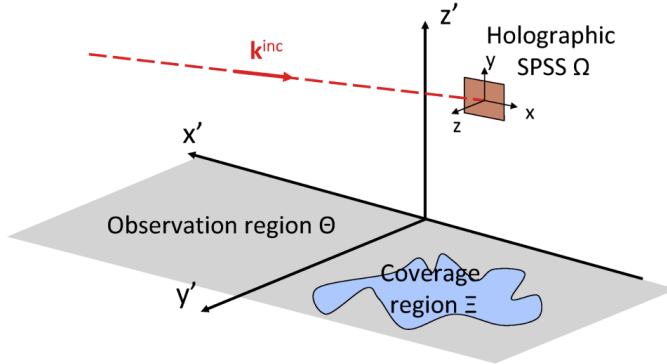


Figure 2.1: Problem geometry. Sketch of the Smart EM skin scenario illustrating the incident wave vector k^{inc} , the observation region Θ , the coverage region Ξ and the holographic SPSSs area with both local (x, y, z) and global (x', y', z') coordinates.

With reference to the scenario in ?? and without loss of generality, let us consider a *SPSSs* composed by $P \times Q$ meta-film unit cells located at the positions $\{\mathbf{r}_{pq} \in \Omega; p = 1, \dots, P; q = 1, \dots, Q\}$, Ω being the smart skinning aperture/support and illuminated by an incident plane wave impinging from the angular direction $(\theta^{inc}, \varphi^{inc})$ whose associated electric magnetic are

$$\mathbf{E}^{inc}(\mathbf{r}) \triangleq (E_{\perp}^{inc}\hat{\mathbf{e}}_{\perp} + E_{\parallel}^{inc}\hat{\mathbf{e}}_{\parallel}) \exp(-j\mathbf{k}^{inc} \cdot \mathbf{r}) \quad (2.1)$$

and

$$\mathbf{H}^{inc}(\mathbf{r}) \triangleq \frac{1}{\eta_0 k_0} \mathbf{k}^{inc} \times \mathbf{E}^{inc}(\mathbf{r}) \quad (2.2)$$

respectively, \mathbf{k}^{inc} being the incident wave vector

$$\mathbf{k}^{inc} \triangleq -k_0 [\sin(\theta^{inc}) \cos(\varphi^{inc}) \hat{\mathbf{x}} + \sin(\theta^{inc}) \sin(\varphi^{inc}) \hat{\mathbf{y}} + \cos(\theta^{inc}) \hat{\mathbf{z}}] \quad (2.3)$$

while: $\mathbf{r} = (x, y, z)$ is the metasurface local coordinate; k_0 is the free-space wavenumber; η_0 is the intrinsic impedance; $\hat{\mathbf{e}}_{\perp} = \frac{\mathbf{k}^{inc} \times \hat{\mathbf{n}}}{|\mathbf{k}^{inc} \times \hat{\mathbf{n}}|}$ is the perpendicular unit vector; $\hat{\mathbf{e}}_{\parallel} = \frac{\hat{\mathbf{e}}_{\perp} \times \mathbf{k}^{inc}}{|\hat{\mathbf{e}}_{\perp} \times \mathbf{k}^{inc}|}$ is the parallel unit

vector; E_{\perp}^{inc} and E_{\parallel}^{inc} are the corresponding complex-valued coefficients; $\hat{\mathbf{n}}$ is the normal to the smart skin surface; $|\cdot|$ is the vector magnitude operator.

In the far-field, the electric field reflected by the *SPSSs* is given by

$$\mathbf{E}^{FF}(\mathbf{r}) \approx \mathcal{G}[\mathbf{J}^e(\mathbf{r}), \mathbf{J}^m(\mathbf{r})] \triangleq \frac{jk_0}{4\pi} \frac{\exp(-ik_0|\mathbf{r}|)}{|\mathbf{r}|} \times \int_{\Omega} \{\hat{\mathbf{r}} \times [\eta_0 \hat{\mathbf{r}} \times \mathbf{J}^e(\tilde{\mathbf{r}}) + \mathbf{J}^m(\tilde{\mathbf{r}})] \exp(jk_0 \hat{\mathbf{r}} \cdot \tilde{\mathbf{r}})\} d\tilde{\mathbf{r}} \quad (2.4)$$

where $\hat{\mathbf{r}} = \frac{\mathbf{r}}{|\mathbf{r}|}$.

Moreover, the effective equivalent electric/magnetic surface current, $\mathbf{J}^e(\mathbf{r})/\mathbf{J}^m(\mathbf{r})$, is computed according to the *GSTC* as follows:

$$\mathbf{J}^e(\mathbf{r}) = j\omega \mathbf{B}_t^e(\mathbf{r}) - \hat{\mathbf{n}} \times \nabla_t B_n^m(\mathbf{r}) \quad \mathbf{r} \in \Omega \quad (2.5)$$

$$\mathbf{J}^m(\mathbf{r}) = j\omega \mu_0 \mathbf{B}_t^m(\mathbf{r}) + \hat{\mathbf{n}} \times \nabla_t \frac{B_n^e(\mathbf{r})}{\varepsilon_0} \quad \mathbf{r} \in \Omega \quad (2.6)$$

where:

- ε_0 is the free-space permeability
- μ_0 is the free-space permeability
- $\mathbf{B}^e(\mathbf{r}) = \mathbf{B}_t^e(\mathbf{r}) + B_n^e(\mathbf{r})\hat{\mathbf{n}}$ is the electric polarization surface density
- $\mathbf{B}^m(\mathbf{r}) = \mathbf{B}_t^m(\mathbf{r}) + B_n^m(\mathbf{r})\hat{\mathbf{n}}$ is the magnetic polarization surface density

If assumed a local periodicity and considered (sufficiently) symmetric unit cells, those expressions become:

$$\mathbf{B}^e(\mathbf{r}) \approx \sum_{p=1}^P \sum_{q=1}^Q [\varepsilon_0 \bar{\chi}(\mathbf{d}_{pq}) \cdot \mathbf{E}_{pq}^{ave}] \Pi^{pq}(\mathbf{r}) \quad \mathbf{r} \in \Omega \quad (2.7)$$

$$\mathbf{B}^m(\mathbf{r}) \approx \sum_{p=1}^P \sum_{q=1}^Q [\bar{\xi}(\mathbf{d}_{pq}) \cdot \mathbf{H}_{pq}^{ave}] \Pi^{pq}(\mathbf{r}) \quad \mathbf{r} \in \Omega \quad (2.8)$$

where

$$\bar{\chi}(\mathbf{d}_{pq}) \triangleq \sum_{i=x,y,z} \chi_{ii}(\mathbf{d}_{pq}) \hat{i}\hat{i} \quad (2.9)$$

and

$$\bar{\xi}(\mathbf{d}_{pq}) \triangleq \sum_{i=x,y,z} \xi_{ii}(\mathbf{d}_{pq}) \hat{i}\hat{i} \quad (2.10)$$

are the diagonal tensors of the electric and magnetic local surface susceptibilities of the (p, q) -th ($p = 1, \dots, P; q = 1, \dots, Q$) unit cell described by the L -size set

$$\mathbf{d}_{pq} \triangleq \{d_{pq}^{(l)}, l = 1, \dots, L\} \quad (2.11)$$

consisting of the (p, q) -th unit scatterer geometrical/physical descriptors, L being the number of descriptors defining each unit cell, while $\Pi^{pq}(\mathbf{r}) \triangleq \{1 \text{ if } \mathbf{r} \in \Omega_{pq}, 0 \text{ if } \mathbf{r} \notin \Omega_{pq}\}$ is the basis function defined on the (p, q) -th ($p = 1, \dots, P; q = 1, \dots, Q$) cell support $\Omega_{pq} (\sum_{p=1}^P \sum_{q=1}^Q \Omega_{pq} = \Omega)$.

Moreover, $\Psi_{pq}^{ave}(\Psi) = \{\mathbf{E}, \mathbf{H}\}$ is the surface averaged field defined as

$$\Psi_{pq}^{ave} \triangleq \frac{\int_{\Omega_{pq}} [\Psi^{inc}(\mathbf{r}) + \Psi^{ref}(\mathbf{r})] d\mathbf{r}}{2 \times \int_{\Omega_{pq}} d\mathbf{r}} \quad (2.12)$$

where the local reflected electric/magnetic field Ψ^{ref} is given by

$$\Psi^{ref}(\mathbf{r}) = \bar{\bar{\Gamma}}[\bar{\bar{\chi}}(\mathbf{d}_{pq}), \bar{\bar{\xi}}(\mathbf{d}_{pq})] \cdot \Psi^{inc}(\mathbf{r}) \quad (2.13)$$

where $\bar{\bar{\Gamma}}$ is the local reflection tensor

$$\bar{\bar{\Gamma}}[\bar{\bar{\chi}}, \bar{\bar{\xi}}] \triangleq \begin{bmatrix} \Gamma_{\perp\perp} & \Gamma_{\parallel\perp} \\ \Gamma_{\perp\parallel} & \Gamma_{\parallel\parallel} \end{bmatrix} \quad (2.14)$$

According to the above derivation, the design of the holographic *SPSS* able to generate a desidered footprint mask in a *Coverage Region* Ξ can be carried out by solving the following two sub-problems:

- *Sub-Problem 1*

The synthesis of the *ideal/reference* surface currents, $\{[\mathbf{J}^w(\mathbf{r})]^*; w = \{e, m\}\}$, that radiate a far-field pattern $[\mathbf{E}^{FF}(\mathbf{r})]^* = \mathcal{G}\{[\mathbf{J}^e(\mathbf{r})]^*, [\mathbf{J}^m(\mathbf{r})]^*\}$ fitting in Ξ the pattern requirements expressed in terms of lower, $\mathcal{L}(\mathbf{r})$, and upper, $\mathcal{U}(\mathbf{r})$, user-defined footprint power masks

$$\mathcal{L}(\mathbf{r}) \leq |[\mathbf{E}^{FF}(\mathbf{r})]^*|^2 \leq \mathcal{U}(\mathbf{r}) \quad (2.15)$$

- *Sub-Problem 2*

The retrieval of the optimal setup of the *SPSS* descriptors, $\mathcal{D}^{opt} = \{\mathbf{d}_{pq}^{opt}; p = 1, \dots, P; q = 1, \dots, Q\}$, so that the target surface currents computed by substituting 2.7 and 2.8 in 2.5 and 2.6 are as close as possible to the ideal ones, $\{[\mathbf{J}^w(\mathbf{r})]^*; w = \{e, m\}\}$, derived in the *Sub-Problem 1*

$$\mathcal{D}^{opt} = arg\{min_{\mathcal{D}}[v(\mathbf{J}^w(\mathbf{r}); [\mathbf{J}^w(\mathbf{r})]^*)]\} \quad (2.16)$$

where

$$v(\mathbf{J}^w(\mathbf{r}); [\mathbf{J}^w(\mathbf{r})]^*) \triangleq \frac{\sum_{w=\{e,m\}} | | [\mathbf{J}^w(\mathbf{r})]^* - \mathbf{J}^w(\mathbf{r}) | |}{\sum_{w=\{e,m\}} | | [\mathbf{J}^w(\mathbf{r})]^* | |} \quad (2.17)$$

is the surface currents fidelity index, while $\mathcal{D} \triangleq \{\mathbf{d}_{pq}; p = 1, \dots, P; q = 1, \dots, Q\}$ and $| | \cdot | |$ stands for the ℓ_2 -norm operator.

The multi-scale nature of the overall *SPSS*s synthesis is fulfilling macro-scale objectives while acting at the unit-cell level by optimizing the small-scale descriptors of the *SPSS* unit cells, $\{d_{pq}^{(l)}; l = 1, \dots, L; p = 1, \dots, P; q = 1, \dots, Q\}$. To achieve those objectives, both lower and upper bounds are enforced in 2.15 to account for macro-scale “coverage region” and “low interference region” targets, respectively. Moreover, since the vast quantity of descriptors used, $N_{\mathcal{D}} (N_{\mathcal{D}} \triangleq P \times Q \times L)$, the computational complexity of the problem in question is, indeed, very high. The reason optimization issues are not taken into account it’s because all of the previous parameters are defined. It’s worth nothing that the dimension of the smart skin is a crucial factor for lowering or increasing the complexity of the problem.

2.1.3 Synthesis Procedure

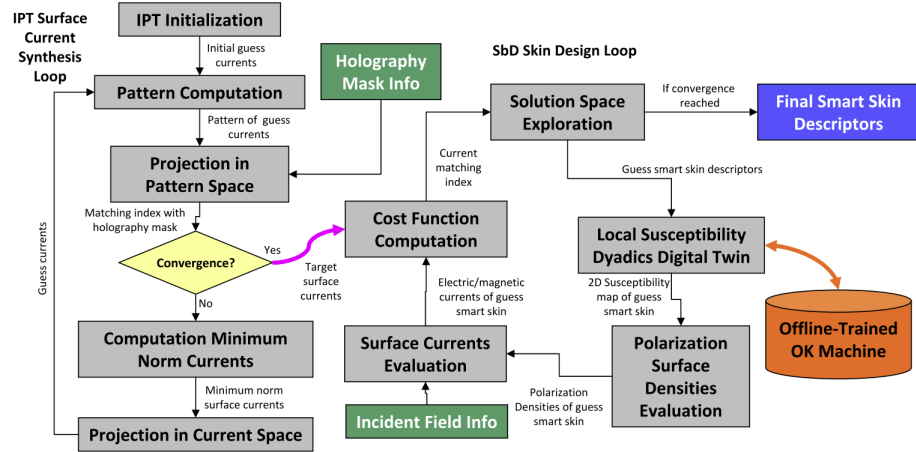


Figure 2.2: SPSS Design Approach. Flowchart of the *IPT-SbD* holographic metasurface synthesis process with details of the elementary blocks and their functional relations.

The problem formulated in ?? needs a combination of *ad-hoc* customized techniques to be solved. In [Salucci.2018](??), is pointed out that the *IS* is affected by ill-posedness, caused by the nonuniqueness of the radiation operator due to the existence of nonradiating currents, which is a problem when the *IS* is concerned with the synthesis of the *ideal* surface currents, $\{\mathbf{J}^w(\mathbf{r})^*; w = \{e, m\}\}$. With that said, it's not doable to directly translate the design method used in [Salucci.2018](??) to *SPSS* case since it purposely made for a “pattern matching objective” and not a “footprint pattern mask constrained” one, such as the one is considered. The need to consider a different solution strategy, inspired by the *IPT*, is absolute.

Firstly, needs to be defined the “pattern” feasible space

$$\mathcal{F}\{\mathbf{E}^{FF}(\mathbf{r})^*\} \triangleq \{\mathbf{E}^{FF}(\mathbf{r})^* : \mathcal{L}(\mathbf{r}) \leq |\mathbf{E}^{FF}(\mathbf{r})^*|^2 \leq \mathcal{U}(\mathbf{r}); \mathbf{r} \in \Xi\} \quad (2.18)$$

and the “current” feasible space

$$\mathcal{F}\{\mathbf{J}^w(\mathbf{r})^*\} \triangleq \{\mathbf{J}^w(\mathbf{r})^* : \mathbf{J}^w(\mathbf{r})^* = C^w \exp[j\psi^w(\mathbf{r})]; \mathbf{r} \in \Omega\} \quad (2.19)$$

where C^w and $\psi^w(\mathbf{r})$ are, respectively, the constant magnitude and profile of the locally-controlled phase of the w -th ($w = \{e, m\}$) current component.

Despite the fact that different scenarios and assumptions can be made while defining the feasibility spaces aforementioned, the 2.19 clearly implies that the *SPSSs* unit cells do not allow a control of the local magnitude of the electric/magnetic currents. Having done all of the required assumption, we are able to implement the *IPT*-based design of the *SPSS* currents design (2.2) accordingly to the following iterative procedure ($h = 1, \dots, H$ being the iteration index) :

- **Initialization ($h=0$):**

The w -th ($w = \{e, m\}$) surface current is discretized

$$\mathbf{J}_h^w(\mathbf{r}) = \sum_{p=1}^P \sum_{q=1}^Q [(J_h^w)_x^{pq} \hat{\mathbf{x}} + (J_h^w)_y^{pq} \hat{\mathbf{y}}] \Pi^{pq}(\mathbf{r}) \quad (2.20)$$

the expansion coefficients, $\{(J_h^w)_x^{pq}; p = 1, \dots, P; q = 1, \dots, Q\}$ and $\{(J_h^w)_y^{pq}; p = 1, \dots, P; q = 1, \dots, Q\}$ being set to random values such that the condition $|(J_h^w)_x^{pq} \hat{\mathbf{x}} + (J_h^w)_y^{pq} \hat{\mathbf{y}}| = C^w (p = 1, \dots, P; q = 1, \dots, Q)$ holds true;

- **Pattern Computation:**

The far-field pattern $\mathbf{E}_h^{FF}(\mathbf{r})$ is evaluated in the coverage region Ξ by substituting 2.20 in 2.4;

- **Projection to Pattern Feasibility Space:**

The projected pattern $\tilde{\mathbf{E}}_h^{FF}(\mathbf{r})$ is obtained by setting

$$\begin{cases} \sqrt{\mathcal{U}(\mathbf{r})} & \text{if } |\mathbf{E}_h^{FF}(\mathbf{r})|^2 > \mathcal{U}(\mathbf{r}) \\ \sqrt{\mathcal{L}(\mathbf{r})} & \text{if } |\mathbf{E}_h^{FF}(\mathbf{r})|^2 < \mathcal{L}(\mathbf{r}) \\ \mathbf{E}_h^{FF}(\mathbf{r}) & \text{otherwise} \end{cases} \quad (2.21)$$

- **Convergence Check:**

The algorithm is terminated by returning the ideal/reference w -th ($w = \{e, m\}$) surface current, $[\mathbf{J}^w(\mathbf{r})]^* = \mathbf{J}_h^w(\mathbf{r})$, if $h = H$ or the *pattern matching index*, χ_h ,

$$\chi_h = \frac{\int_{\Xi} |\tilde{\mathbf{E}}_h^{FF}(\mathbf{r}) - \mathbf{E}_h^{FF}(\mathbf{r})|^2 d\mathbf{r}}{\int_{\Xi} |\mathbf{E}_h^{FF}(\mathbf{r})|^2 d\mathbf{r}} \quad (2.22)$$

satisfies the condition $\chi_h \leq \chi^*$, χ^* being a user-chosen convergence threshold;

- **Computation of Minimum Norm Currents:**

Compute the *minimum norm* component of the w -th ($w = \{e, m\}$) surface current, $[\mathbf{J}_h^w(\mathbf{r})]^{MN}$ (MN means *minimum norm*), by solving 2.4 with respect to the currents. Towards this end, the method based on the truncated singular value decomposition, detailed in [Salucci.2018](??), is applied;

Projection to Current Feasibility Space:

Update the iteration index ($h \leftarrow h + 1$) and evaluate the w -th $w = \{e, m\}$ projected surface current $\mathbf{J}_h^w(\mathbf{r})$

$$\mathbf{J}_h^w(\mathbf{r}) = C^w \times \sum_{p=1}^P \sum_{q=1}^Q \frac{[(J_{h-1}^w)_x^{pq}]^{MN} \hat{\mathbf{x}} + [(J_{h-1}^w)_y^{pq}]^{MN} \hat{\mathbf{y}}}{\|[(J_{h-1}^w)_x^{pq}]^{MN} \hat{\mathbf{x}} + [(J_{h-1}^w)_y^{pq}]^{MN} \hat{\mathbf{y}}\|} \Pi^{pq}(\mathbf{r}) \quad (2.23)$$

Restart process from the “**Pattern Computation**” step.

Once the reference surface currents, $\{\mathbf{J}^w(\mathbf{r})\}^*; w = \{e, m\}\}$, have been found, the *Sub-problem 2* is then addressed by solving 2.16. More precisely, an iterative *SbD*-based strategy inspired is customized to the problem at hand by implementing the following blocks of the functional flowchart in 2.2:

1. the “**Solution Space Exploration (SSE)**” block aimed at optimizing the *SPSS* descriptors by defining a succession of S iterations (s being the *SbD* iteration index, $s = 1, \dots, S$) where G trial solutions, $\{\mathcal{D}_g^{(s)}; g = 1, \dots, G\}, \mathcal{D}_g^{(s)} \triangleq \{\mathbf{d}_{pq}|_g^{(s)}; p = 1, \dots, P; q = 1, \dots, Q\}$ being the g -th trial at the s -th iteration, evolve towards the global solution $\mathcal{D}^{opt} 2.16$. As said before, being the nature of the problem at hand ill-posed, and considering the non-linear function to be optimized, a global search mechanism based on the *Particle Swarm Optimizer (PSO)*¹ has been chosen to update/evolve the population of trial solutions at each s -th ($s = 1, \dots, S$) step, $\mathcal{D}^{(s)}$;
2. the “**Cost Function**” (*CF*) evaluation block that implements the discretized version of 2.16;
3. the “**Surface Current Evaluation**” (*SCE*) block that employs 2.5 and 2.6 to determine $\mathbf{J}^w(\mathbf{r})$ starting from $\mathbf{B}^w(\mathbf{r}), w = \{e, m\}$;
4. the “**Polarization Surface Densities Evaluation**” (*PSDE*) block that implements 2.7 and 2.8 to yield the w -th ($w = \{e, m\}$) polarization surface density, $\mathbf{B}^w(\mathbf{r})$;

¹PSO method

Is a computational method that optimizes a problem by iteratively trying to improve a candidate solution with regard to a given measure of quality

5. the “Local Susceptibility Dyadics Digital Twin” (*LSDDT*) block devoted to determine $\bar{\chi}(\mathbf{d}_{pq}|_g^{(s)})$ and $\bar{\xi}(\mathbf{d}_{pq}|_g^{(s)})$ to be used in the *PSDE* block to compute the polarization surface densities at each s -th ($s = 1, \dots, S$) iteration for each g -th ($g = 1, \dots, G$) guess solution in each (p, q) -th ($p = 1, \dots, P; q = 1, \dots, Q$) unit cell of the *SPSS*.

As for the last point treated and analogously to the unit cell of reflectarrays, each susceptibility tensor set, $\bar{\chi}(\mathbf{d}_{pq}|_g^{(s)})$ and $\bar{\xi}(\mathbf{d}_{pq}|_g^{(s)})$, generated in the *SbD* iterative process, is full-wave evaluated; the result is computationally unfeasible, since this would require the numerical modelling and the full-wave solution of $P \times Q \times G \times S$ *SPSSs*. With that said, the dyadics, $\bar{\chi}(\mathbf{d})$ and $\bar{\xi}(\mathbf{d})$, are approximated with their surrogate $\bar{\chi}'(\mathbf{d})$ and $\bar{\xi}'(\mathbf{d})$, as the (*DT*) states, which is implemented according to a statistical learning approach based on the *Ordinary Kriging (OK)*² method starting from a set of A full-wave computed unit cell responses $[\mathbf{d}_a; \bar{\chi}(\mathbf{d}_a); \bar{\xi}(\mathbf{d}_a)], a = 1, \dots, A$. Since the *OK* is capable of effectively creating reliable and accurate surrogate models of wave manipulating devices, its choice is obvious.

Since, in [Yang.2021](??) has been computed $\bar{\chi}(\mathbf{d}_a), \bar{\xi}(\mathbf{d}_a)$, starting from the full-wave simulation of the unit cell reflection matrix under local periodicity assumption $\bar{\Gamma}(\mathbf{d}_a)$ and retrieving the associated dyadics by standard inversion formulas such as

$$\xi_{xx}(\mathbf{d}_a) = \frac{2j \Gamma_{\perp\perp}(\mathbf{d}_a) + 1}{k_0 \Gamma_{\perp\perp}(\mathbf{d}_a) - 1} \quad (2.24)$$

which is valid for reflecting cells (in [Yang.2021](??), Chapter 3, the author has computed this application on other components).

It is worth considering the fact that the *DT* has to predict the local susceptibility tensor rather than the local reflection coefficient, since the reflectarray case is not experimented. This means that 6 complex coefficients (adding $\bar{\chi}(\mathbf{d})$ and $\bar{\xi}(\mathbf{d})$ to the count) are computed, instead of 4 terms, deriving from the reflection matrix. This implies that the *DT* of a *SPSS* can neglect the incidence angle of the illuminating field since the susceptibility tensor does not depend on it, unlike what has been treated in [Yang.2021]??.

Since have been treated all the aspects of the *IPT-SbD* flowchart, a numerical experimentation will follow this section, considering various footprints, since, as said before, our problem takes in account a “footprint pattern mask” constraint.

2.1.4 Numerical Results

Since the formulation of all the needed formulas, criterias and procedures, has been done, the next step is to numerically resolve the *Sub-Problem 1* and *Sub-Problem 2*, besides the value of the pattern matching index of the *SPSS* final layout, \mathcal{X} 2.22 ,utilizing all the data contained in 2.1³. The data found in 2.1 are quantified by computing the *reference pattern matching* \mathcal{X}^{IPT} ($\mathcal{X}^{IPT} \triangleq \mathcal{X}_H$, referenced in *Sub-Problem 1*) and the *surface current fidelity index* v^{SbD} ($v^{SbD} \triangleq v(\mathbf{J}^w(\mathbf{r})|_{s=S}; [\mathbf{J}^w(\mathbf{r})]^*)$, referenced in *Sub-Problem 2*). The focus of this section is to prove the effectiveness, through the illustration of the *IPT-SbD* design process, for the synthesis of footprint pattern shaped holographic *SPSSs*.

²OK Method

Is a spatial estimation method where the error variance is minimized. It's not dependent on the data used to make the estimate.

³Computational Times

The computational times refer to non-optimized MATLAB serial implementations executed on a single-core laptop running at 1.60 [GHz].

Footprint Name	Footprint Mask	$P \times Q$	Δt^{IPT} [s]	Δt^{SbD} [s]	Δt^{PSO} [s]	χ^{IPT}	v^{SbD}	χ^{SPSS}
<i>Square</i>	Fig. 3(a)	200×200	2.31×10^2	9.30	4.01×10^6	6.44×10^{-4}	2.05×10^{-1}	1.08×10^{-3}
<i>Checkerboard</i>	Fig. 6(a)	200×200	2.37×10^2	9.08	4.00×10^6	5.27×10^{-4}	2.04×10^{-1}	7.78×10^{-4}
<i>IEEE</i>	Fig. 8(b)	200×200	1.89×10^2	8.82	4.01×10^6	3.65×10^{-3}	2.06×10^{-1}	4.84×10^{-3}
<i>ELEDIA</i>	Fig. 8(c)	25×25	1.22×10^2	1.64×10^{-1}	6.26×10^4	5.70×10^{-3}	2.11×10^{-1}	6.55×10^{-3}
<i>ELEDIA</i>	Fig. 8(c)	50×50	1.46×10^2	6.20×10^{-1}	2.50×10^5	2.21×10^{-3}	2.07×10^{-1}	2.72×10^{-3}
<i>ELEDIA</i>	Fig. 8(c)	100×100	1.53×10^2	2.45	1.02×10^6	1.22×10^{-3}	2.03×10^{-1}	1.55×10^{-3}
<i>ELEDIA</i>	Fig. 8(c)	150×150	1.64×10^2	6.35	2.25×10^6	5.97×10^{-4}	2.04×10^{-1}	8.15×10^{-4}
<i>ELEDIA</i>	Fig. 8(c)	200×200	2.66×10^2	9.31	4.01×10^6	3.70×10^{-4}	2.07×10^{-1}	5.65×10^{-4}
<i>ELEDIA</i>	Fig. 8(c)	400×400	1.03×10^3	3.61×10^1	1.61×10^7	1.92×10^{-4}	2.05×10^{-1}	3.38×10^{-4}

Table 2.1: Numerical Validation, Matching and Computational Indexes

The benchmark SEE scenario is modeled after this features:

- Base Station that illuminates from $(\theta^{inc}, \varphi^{inc}) = (20, 105)[\text{deg}]$;
 - Linearly-Polarized plane wave with a $+45[\text{deg}]$ slant polarization at $f = 30[\text{GHz}]$
 - Different *SPSS* apertures and target footprint masks
 - The metasurface unit cell, which consists of a square passive and static metallic patch, with periodicity $\delta_x = \delta_y = 5.0 \times 10^{-3}[\text{m}]$, printed on a single-layer substrate (Rogers 3003 dielectric with thickness $\tau = 5.08 \times 10^{-4}[\text{m}]$) has been used ($L = 1$) and modelled in *HFSS* for generating/training the *LSDDT* block.
- A simple yet efficient structure has been chosen to highlight the potentials of the *IPT-SbD* strategy, even when dealing with elementary unit cells which feature an inexpensive fabrication process since: only one dielectric layer is employed, the metalization contour complexity is very limited and no via holes are present;
- The following *IPT-SbD* based parameters has been chosen ⁴: $H = 10^3$, $\chi^* = 10^{-4}$, $S = 10^4$ and $G = 10$.

“Square” Footprint Experiment

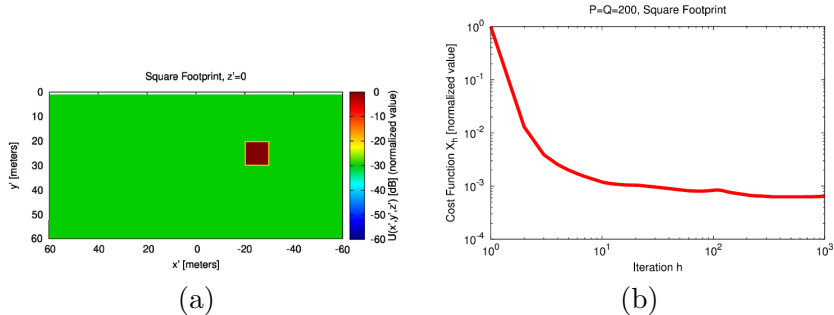


Figure 2.3: Numerical Validation (“Square” Footprint, $P = Q = 200$) - Plot of (a) the footprint pattern mask $[U(\mathbf{r}'); \mathbf{r}' \in \Theta]$ and (b) evolution of the *IPT* cost function versus the iteration index, $h(h = 1, \dots, H)$.

The first proposed footprint pattern is a $P \times Q = 200 \times 200$ holographic *SPSS* with an $1 \times 1[\text{m}]$ support Ω , as explained in ??, located at the position $(x', y', z') = (0, 0, 15)[\text{m}]$ in the global coordinate system. The upper and lower masks have been defined so that the skin reflect a constant-power square footprint in the coverage region Ξ of lateral size $10[\text{m}]$ centered at $(x', y', z') = (-25, 25, 0)[\text{m}]$ [”Square Footprint” - 2.3(a)], while a $-30[\text{dB}]$ footprint power reduction has been enforcer outside Ξ in the observation region Θ of extension $120 \times 60[\text{m}^2]$.

As seen in 2.3(b), the evolution on the *IPT* cost function (modelled after the steps solved in the *IPT*-based iterative procedure in 2.1.3), there is a quick minimization and a convergence to a solution

⁴??

As stated in [Yang.2021] (and in all citated papers inside), the following parameters has been chosen through *deterministic and stochastic* optimization techniques.

with a very small mismatch from the target footprint pattern, $\mathcal{X}_H = 6.44 \times 10^{-4}$ in less than 4 minutes 2.1 thanks to the exploitation of a fast Fourier transformarm within the *IPT* loop despite the huge number of unknowns.

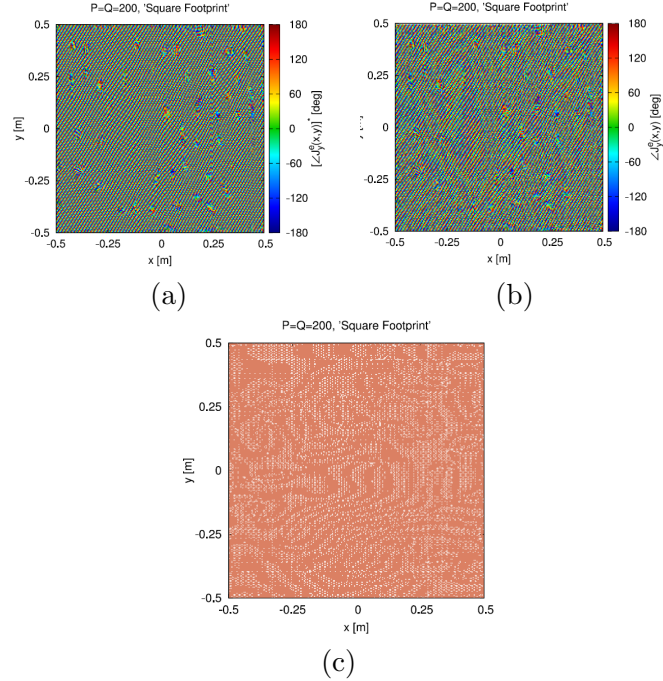


Figure 2.4: Numerical Validation (“Square” Footprint, $P = Q = 200$) - Plot of the phase distribution of (a) the *IPT*-reference/ideal current along with (b) that generated by the synthesized *SPSS* layout (c).

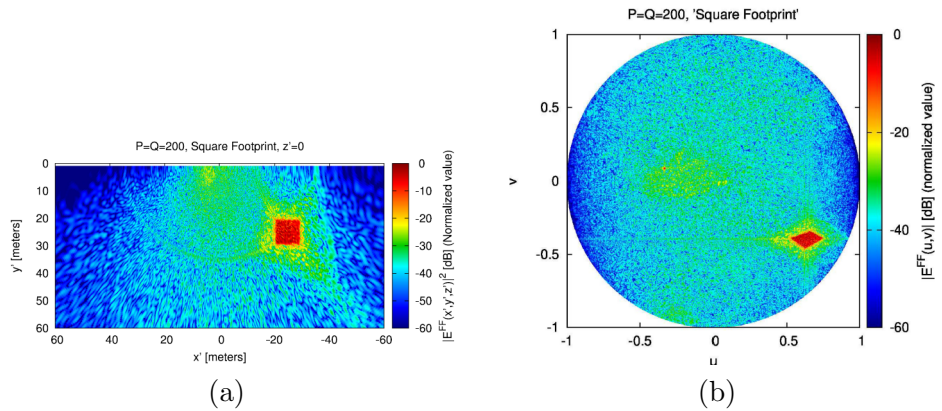


Figure 2.5: Numerical Validation (“Square” Footprint, $P = Q = 200$) - Plots of the radiated (a) footprint pattern within the observation region Θ and (b) angular power distribution.

Proceeding to the *Sub-Problem 2*, the *SbD* optimization process quickly ($\Delta t^{SbD} < 10[s]$ - 2.1) yields, thanks to an accurate matching with the reference current [2.4(a) vs. 2.4(b)], a final layout [2.4(c)] that faithfully fulfills the mask requirements as pictorially confirmed by the plot of the radiated footprint pattern within the observation region [2.5(a) vs. 2.3(a)].

As seen from the data in 2.1, the time using the *IPT*-based process versus the time using the *PSO*-driven optimization is significantly lower [Δt^{IPT} vs. Δt^{PSO}], remarking the efficiency of the synthesis procedure detailed in 2.1.3.

Another point worth noting is the “focusing” skill of the *SPSS* seen in 2.5(c): as seen, the synthesized *SPSS* has the ability to compensate the angular beam distortion caused by the position and the orientation of the coverage region, with respect to the smart skin and the incident wave. As expected,

in a real-life environment, it's crucial for the smart skin to be able to compensate such error, otherwise the need for the *IPT-SbD* based process it's unnecessary. This will expanded further in the ?? section, with reference to all other experiments.

“Checkerboard”, “IEEE” and “ELEDIA” Footprint Experiment

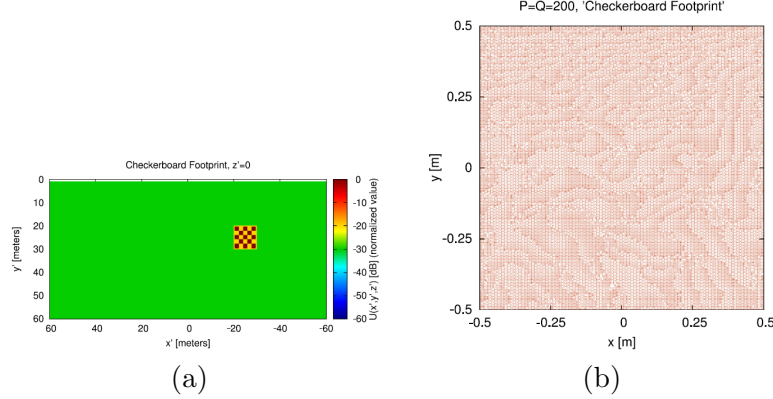


Figure 2.6: Numerical Validation (“*Checkerboard*” Footprint, $P = Q = 200$) - Plot of (a) the footprint pattern mask $[\mathcal{U}(\mathbf{r}'); \mathbf{r}' \in \Theta]$ and (b) layout of the synthesized *SPSS*.

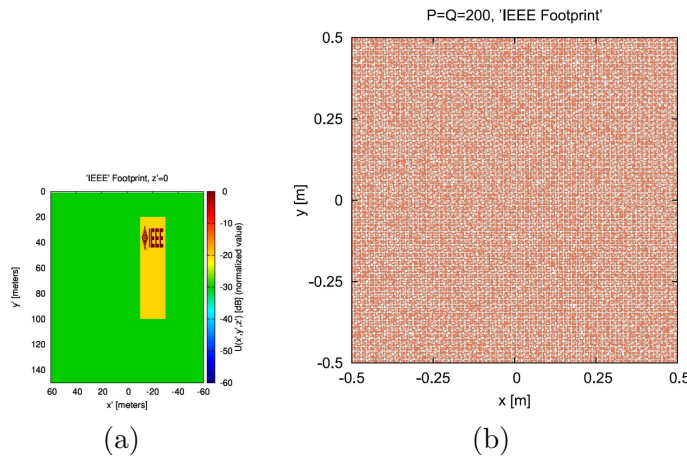


Figure 2.7: Numerical Validation (“*IEEE*” Footprint, $P = Q = 200$) - Plot of (a) the footprint pattern mask $[\mathcal{U}(\mathbf{r}'); \mathbf{r}' \in \Theta]$ and (b) layout of the synthesized *SPSS*.

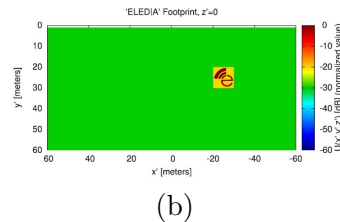


Figure 2.8: Numerical Validation (“*ELEDIA*” Footprint, $P = Q$ have various values) - Plot of (a) the footprint pattern mask $[\mathcal{U}(\mathbf{r}'); \mathbf{r}' \in \Theta]$.

As seen, the footprint mask just show are more complex than the one before. But, is worth nothing that the change in complexity of the footprint masks don't impact on the *CPU* time for synthesis process nor on the convergence of the two-step synthesis. Taking in example the “*Checkerboard*” footprint, the difference is shown as follows in Table (2.2):

	“Square”	“Checkerboard”
$\Delta t^{IPT}[s]$	2.31×10^2	2.37×10^2
$\Delta t^{SbD}[s]$	9.30	9.08
χ^{SPSS}	1.08×10^{-3}	7.78×10^{-4}
v^{SbD}	2.05×10^{-1}	2.04×10^{-1}

Table 2.2: Computational difference between footprints

As can be seen in the 2.7, it's worth noting for the sake of the experiment, that even a complex-built footprint mask can be used and perform in a matter of real-life utilization; the pattern can be seen in Table2.9:

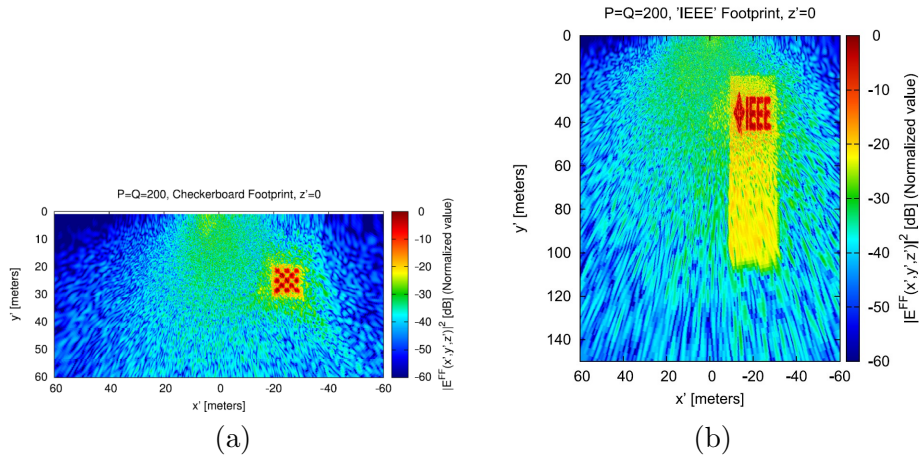


Figure 2.9: Numerical Validation (“Checkerboard” and “IEEE” Footprint, $P = Q = 200$) - Plots of the radiated (a) “Checkerboard” footprint pattern and (b) “IEEE” footprint pattern within the observation region Θ .

The “IEEE” footprint pattern is modeled with a rectangle of $20 \times 80[m]$ in front of the smart skin, which increases the local-complexity of the footprint.

Until now, it's been experimented with “fixed” dimension masks; but there is the need to verify if the *IPT-SbD* process for various mask dimensions.

This experiment is going to be verified by introducing an “ELEDIA” footprint mask, with dimensions varying from $P = Q = 50$ to $P = Q = 400$.

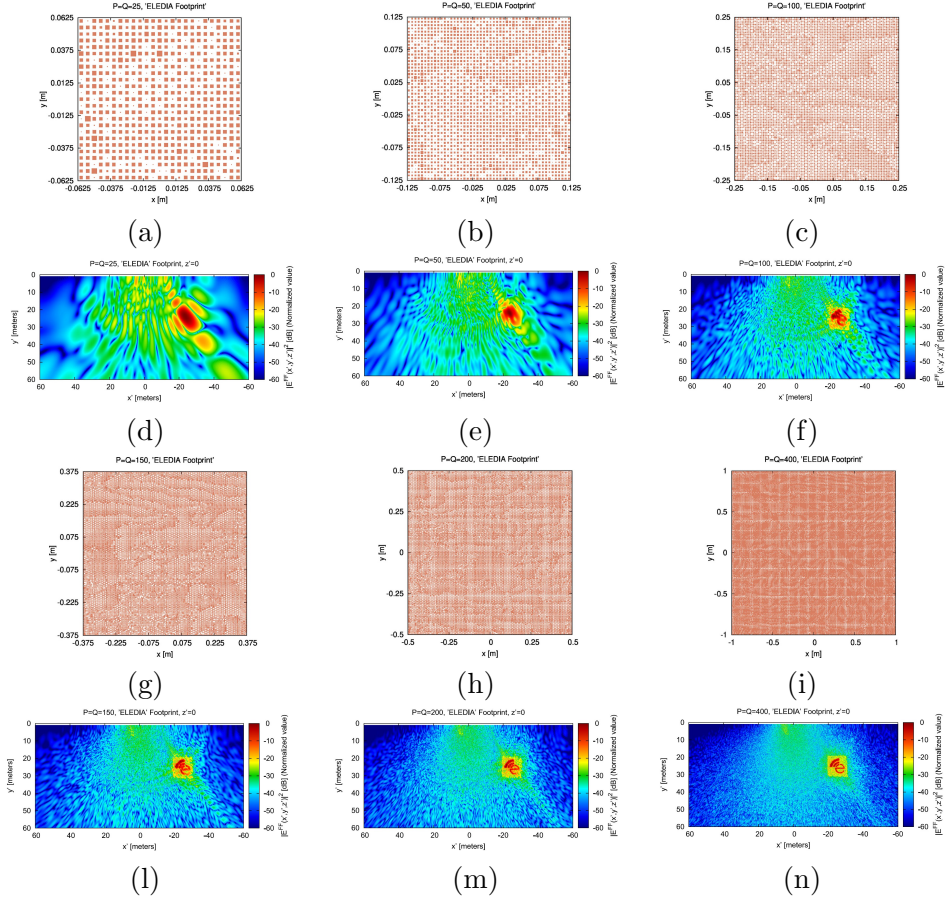


Figure 2.10: Numerical Validation (“ELEDIA” Footprint) - Layout of synthesized SPSS (First and Third Column) and footprint patterns radiated in the observation region Θ (Second and Forth Column) by the SPSS when $P = Q = 25, 50, 100, 150, 200, 400$.

As seen from Fig.2.10, the more unit cells we have, P and Q , the more precise the footprint pattern is going to be.

With the help of the figures from 2.6, 2.7, 2.9 and 2.10, we can address the cost functions:

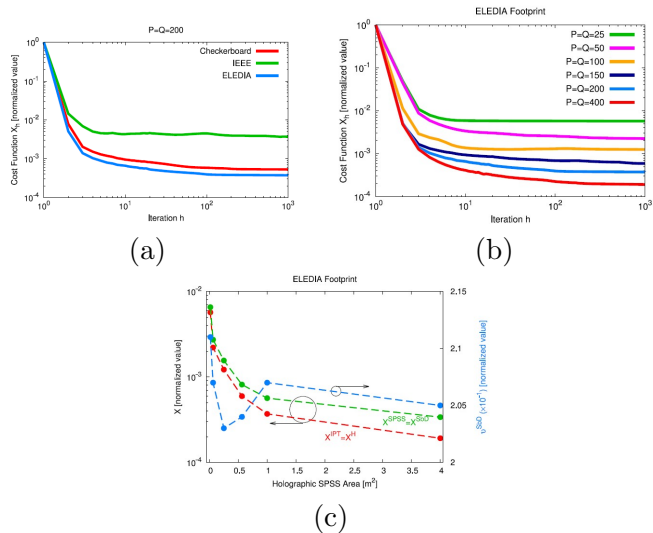


Figure 2.11: Numerical Validation (“Checkerboard”, “IEEE” and “ELEDIA” footprints) - Plot of (a) the evolution of the IPT cost function for between the three kinds of footprints, (b) the evolution fo the IPT cost function for all “ELEDIA” footprints and (c) the matching indexes [$\mathcal{X}^{SPSS} = \mathcal{X}^{SbD}$ (green line), v^{SbD} (blue line) and \mathcal{X}^{IPT} (red line)] versus the SPSS size.

Chapter 3

Planning EM

3.1 Introduction

As stated in the previous section, improving the quality of service is crucial in an urban environment. Thus follows the reason behind the following work: planning a SEE using a single or combined EMSs to improve the quality of service in specific areas. To achieve the stated goal, the EMSs are going to be shaped using a Unit Cell adapted for every chosen spot. In the following discourse, various EMSs are going to be strategically shaped and placed to fit the SEE that needs improving. All of the following described steps are going to be applied for every ROI in the same way, adjusting just the quantity of EMSs and the characteristics for every EMS.

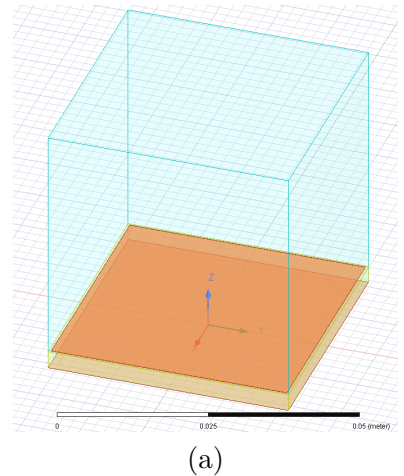
3.2 Scenario

3.2.1 Parameters

- Dimensions of scenario: $D_x = D_y = 1500[m]$
- Resolution: $\Delta_x = \Delta_y = 5[m]$
- BTS Position: $r_\Psi = (850, 850, 30)[m]$
- BTS Power: $P_{TX} = 20[W]$
- BTS Sectors: 3
- BTS Azimuth Angular Extension: $\Delta\phi = 120[deg]$
- Spacing: $\lambda/2$

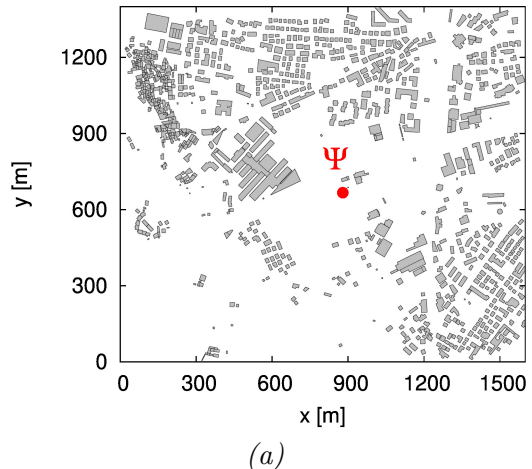
Scenery Presentation

The first step is to define and model the scenario.



(a)

Figure 3.1: (a) - Unit Cell modelled in HFSS



(a)



Figure 3.2: (a) Scenario in WinProp - (b) Scenario in OpenStreetMap - (c) Scenario in GoogleMaps

3.2.2 Power and Threshold

Analyzing the radiaton pattern and thresholded pattern is needed to find weak spots inside the scenario.

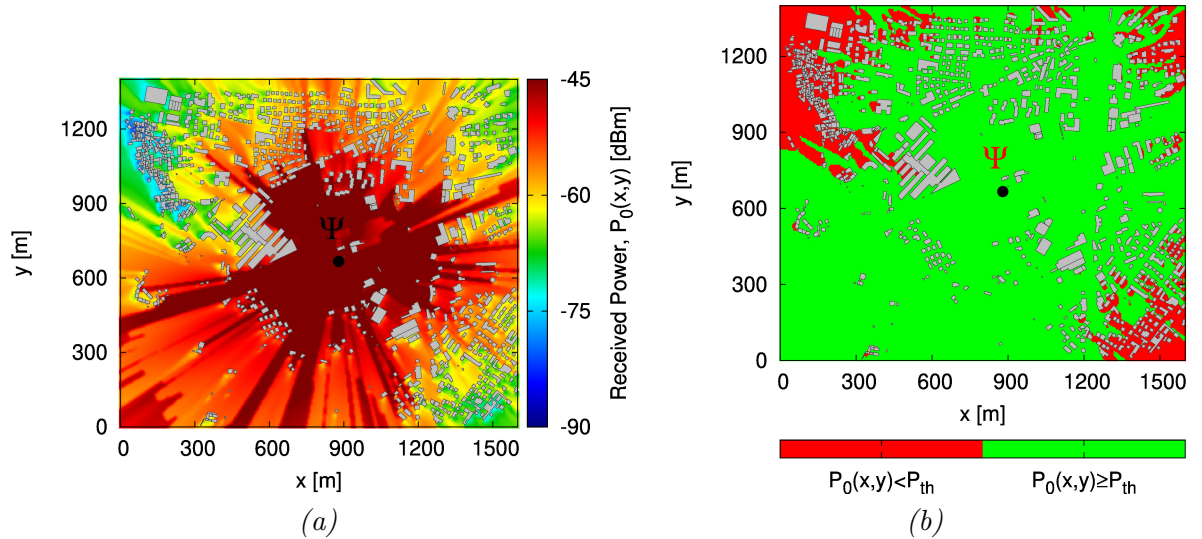


Figure 3.3: (a) Irradiated Power in Scenario - (b) Thresholded power at $-65[dB]$ in scenario

3.2.3 Region of Interest

Having chosen and modeled the scenario, the Regions of Interest, or “RoIs”, needs to be found.

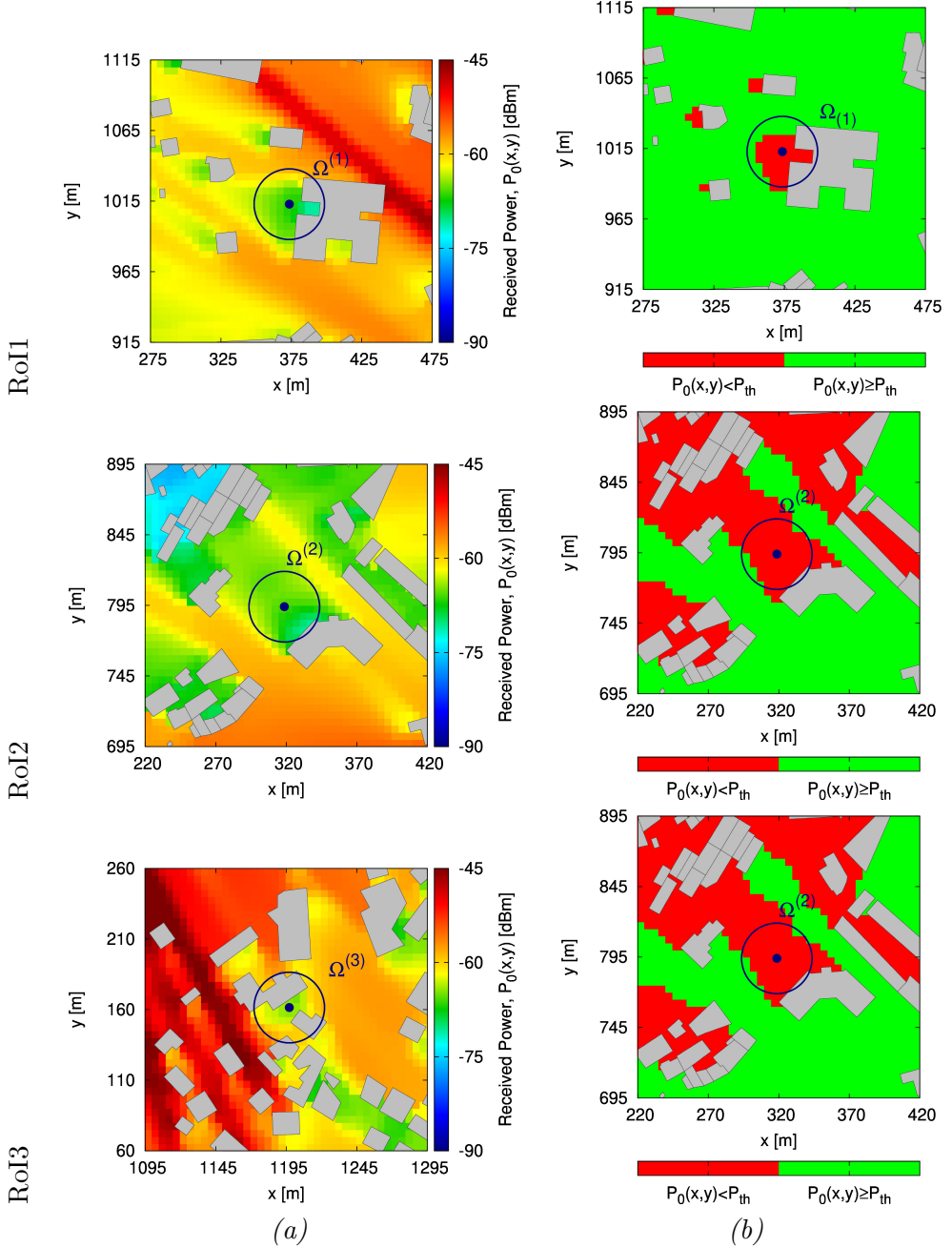


Figure 3.4: (a) Nominal Power for selected Region of Interest - (b) Thresholded power at $-65[\text{dB}]$ for selected Region of Interest

The following weak spots have been found, meaning that these spots perform badly under $-65[\text{dBm}]$, which is the thresholded value used in this discourse to determine if the BTS is working as supposed to. It is crucial to maintain the signal above the threshold, otherwise the BTS, and thus the ISP that owns the BTS, is incapable to provide a minimum quality for the service, meaning that the user is going to be affected. For example, the streaming video that the user is watching will lag quite a bit if the received power in that zone is below $-65[\text{dBm}]$. On the other hand, choosing spots with received power way above the threshold is a waste of resources, since it's not needed to analyze, model and test a EMS to improve said spot.

3.2.4 Smart Skins Choice

After defining the weak spots, or "Region of Interest", the following step is to determine which wall is best suited to having a EMS applied to it. Two criterias are mainly used for this step: the proximity from the RoI, which the maximum value is ca. 70 meters, and the Incident Power on said wall, which should be at least above 80 dB mu V/m, even though it's best to have it over 90 to ensure a good

amount of power reflected.

Afterwards, when every ROI is deeply examined, all of the ROI characteristics are going to be listed, showing the meaning behind the selection.

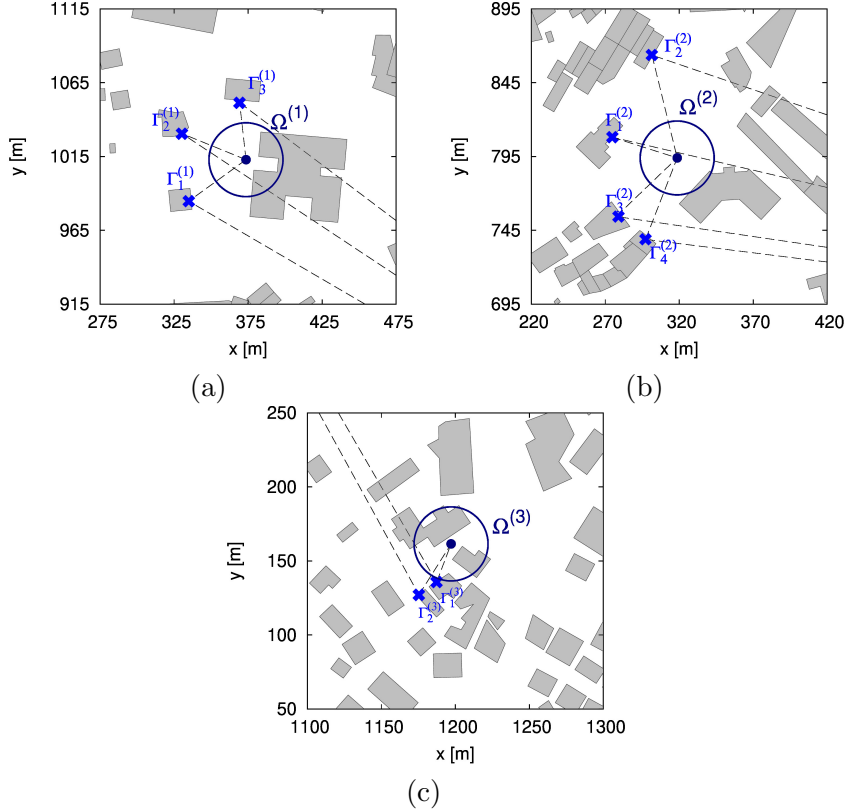


Figure 3.5: (a) Smart Skin Choice for Region Of Interest 1 - (b) Smart Skin Choice for Region Of Interest 2 - (c) Smart Skin Choice for Region Of Interest 3

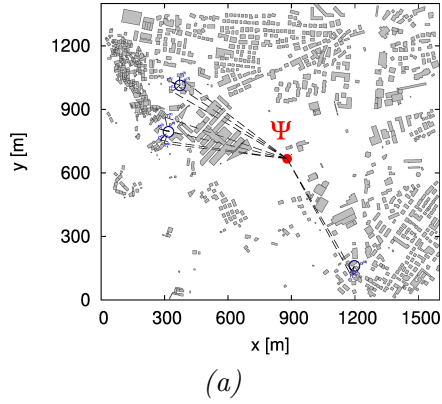


Figure 3.6: (a) Cumulative Smart Skin Choices

3.2.5 Enhancement Region of Interest 1

After defining all the characteristichs of the ROI, the next step is to model the EMS, using the incident angles and the reflected angles. The layout and the directivity of each EMS is shown, providing a view of the direction which the EMS is intended to work.

Smart Skin Sizing and Layout

#	$\Gamma_1^{(1)}$	$\Gamma_2^{(1)}$	$\Gamma_3^{(1)}$
Shape	Square	Square	Square
EMS Side	$d = 2[m]$	$d = 2[m]$	$d = 2[m]$
Number elements along x	$N_x = 50$	$N_x = 50$	$N_x = 50$
Number elements along y	$N_y = 50$	$N_y = 50$	$N_y = 50$
Distance from BTS	$D_\Psi = 639.23[m]$	$D_\Psi = 658.91[m]$	$D_\Psi = 627.85[m]$
Distance from RoI1	$D_\Omega = 40.26[m]$	$D_\Omega = 39[m]$	$D_\Omega = 47.04[m]$
Incident angle	$(\theta_i, \phi_i) = (57.33, 1.60)[deg]$	$(\theta_i, \phi_i) = (16.72, 4.54)[deg]$	$(\theta_i, \phi_i) = (34.02, 177.55)[deg]$
Reflection angle	$(\theta_r, \phi_r) = (20.23, -104.13)[deg]$	$(\theta_r, \phi_r) = (30.67, -42.74)[deg]$	$(\theta_r, \phi_r) = (49.47, -22.18)[deg]$
EMS Location	$(x_\Gamma, y_\Gamma, z_\Gamma) = (334, 979, 15)[m]$	$(x_\Gamma, y_\Gamma, z_\Gamma) = (330, 1030, 15)[m]$	$(x_\Gamma, y_\Gamma, z_\Gamma) = (369, 1051, 15)[m]$
Incident field strength	$E_{rms} = 89.47[dB\mu V/m]$	$E_{rms} = 86.26[dB\mu V/m]$	$E_{rms} = 96.49[dB\mu V/m]$
Reflected power	$P_T = -20.27[dBm]$	$P_T = -19.42[dBm]$	$P_T = -13.76[dBm]$

Table 3.1: Region of Interest 1 data

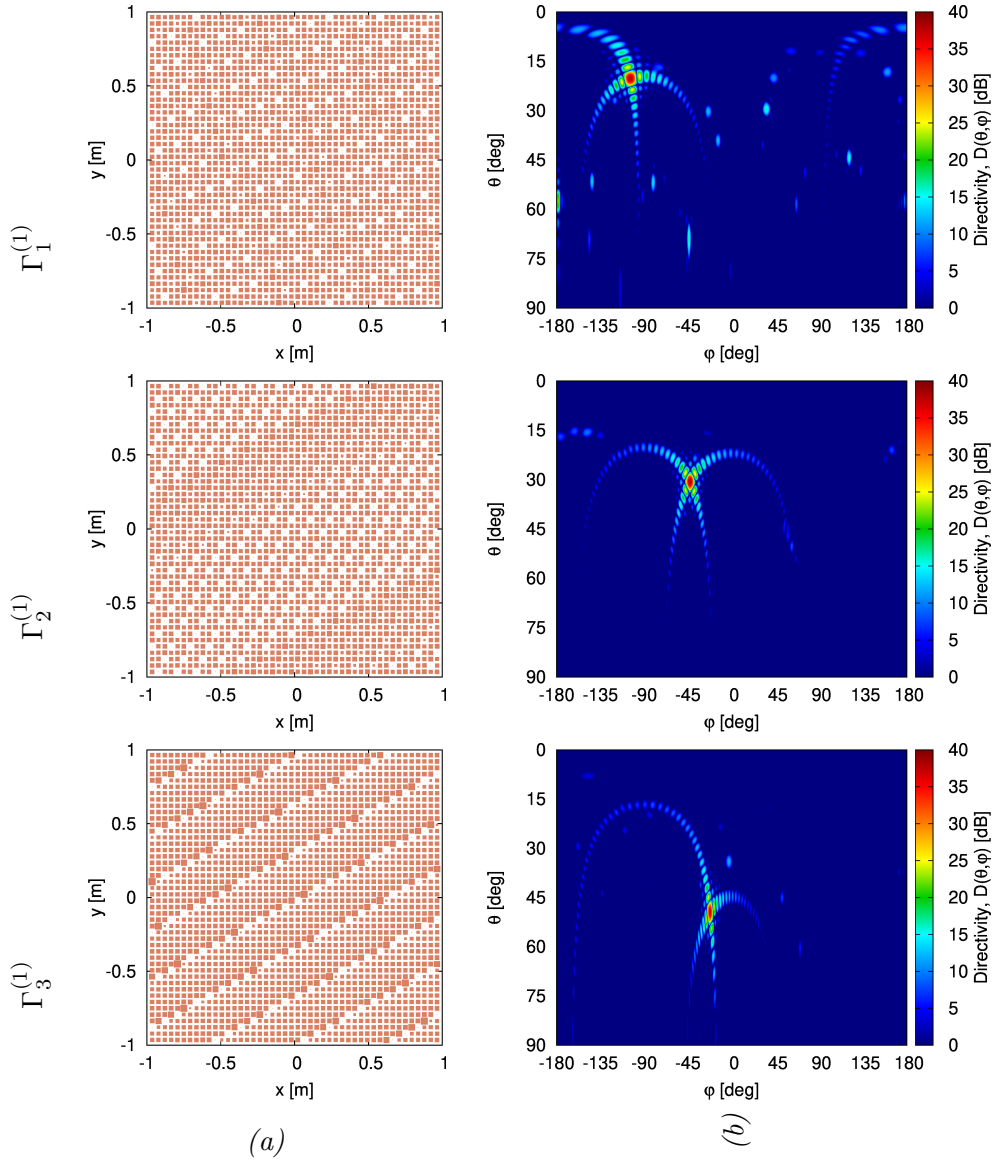


Figure 3.7: (a) Layout - (b) Directivity

Smart Skin Performance

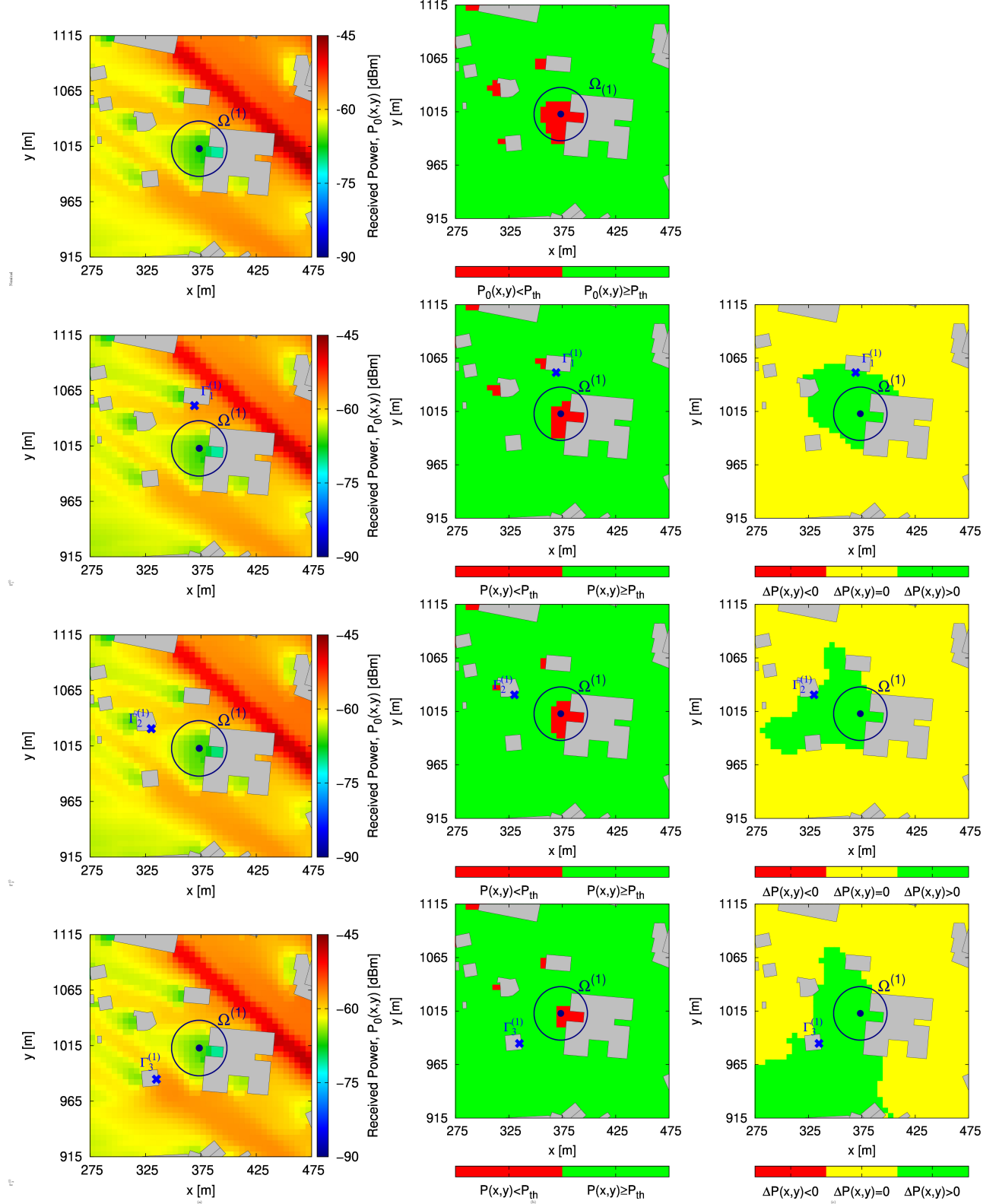


Figure 3.8: (a) Nominal BTS Power Performance vs Smart Skin Performance in Region of Interest 1 - (b) (a) Nominal BTS Thresholded Power Performance vs Thresholded Smart Skin Performance in Region of Interest 1 - (c) Difference between received and reflected power thresholded at -65 [dBm]

Having applied the modelled EMSs in each intended spot, it's clear that an improvement has been made, especially with $\Gamma_3^{(1)}$, which is going to be chosen as best performing EMS.

Best Skin and Overall Implementation

A scenario with all of the EMSs is show, with the thresholded map and the difference between the Reference Scenario and the Improved Scenario.

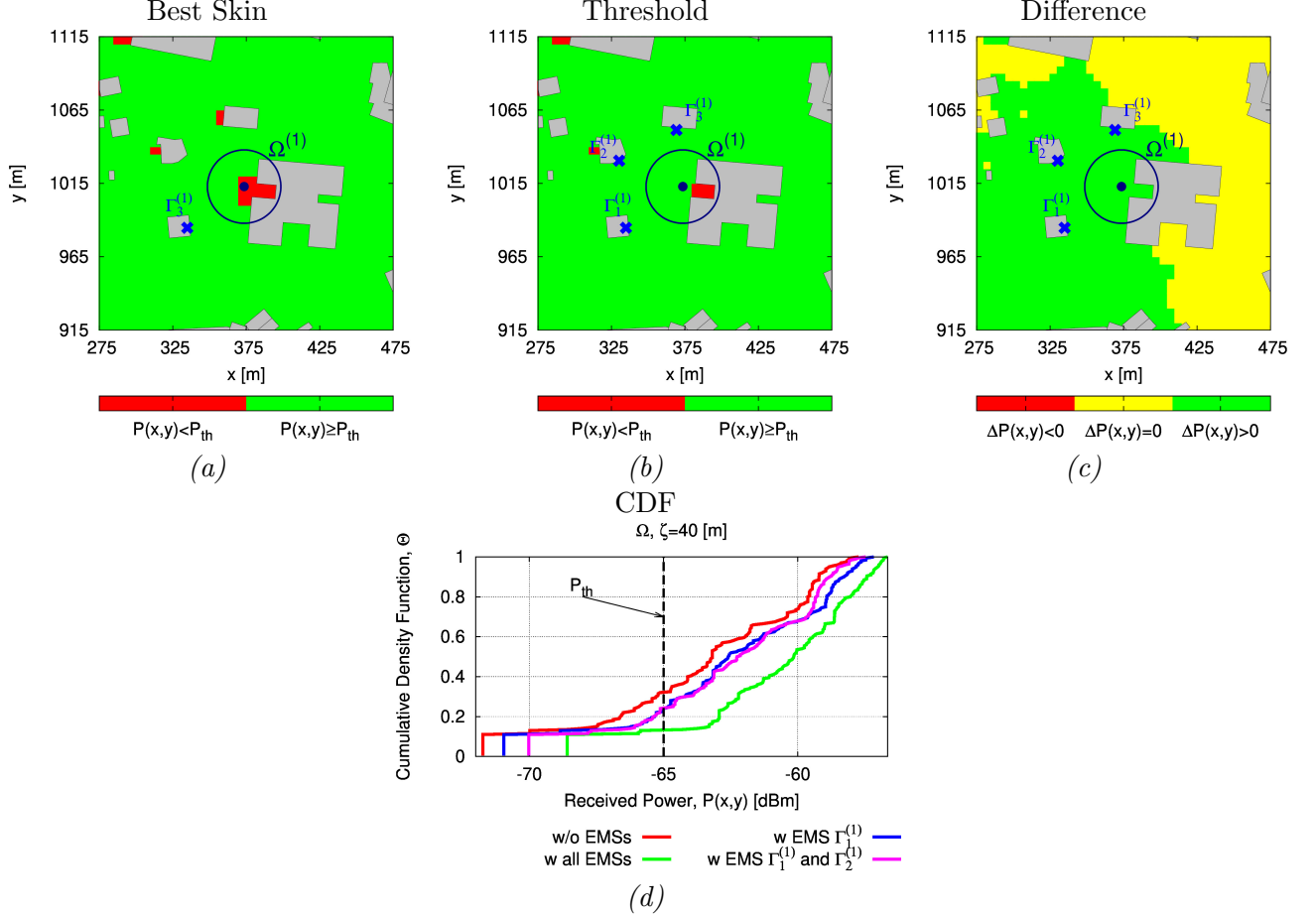


Figure 3.9: (a) - Best Skin for examined Scenario (b) Environment with Smart Skins - (c) Difference between referenced and smart skin implemented Region of Interest - (d) Cumulative Density Function [-65dBm]

The difference between Referenced and EMSs implemented RoI is very useful, not only to see the improvement in the RoI but even in other places surrounding the EMSs.

A graph for the CDF, Cumulative Density Function, is shown, stating the probability that a point inside the RoI is going the threshold value. For example, with all the EMSs applied, the CDF is ca. 17% in the RoI, much better than the referenced scenario, which was ca. 33%.

3.2.6 Enhancement Region of Interest 2

Smart Skin Sizing and Layout

#	$\Gamma_1^{(2)}$	$\Gamma_2^{(2)}$	$\Gamma_3^{(2)}$	$\Gamma_4^{(2)}$
Shape	Square	Square	Square	Square
EMS Side	$d = 2[m]$	$d = 2[m]$	$d = 2[m]$	$d = 2[m]$
Number elements along x	$N_x = 50$	$N_x = 50$	$N_x = 50$	$N_x = 50$
Number elements along y	$N_y = 50$	$N_y = 50$	$N_y = 50$	$N_y = 50$
Distance from BTS	$D_\Psi = 610.74[m]$	$D_\Psi = 621.01[m]$	$D_\Psi = 606.90[m]$	$D_\Psi = 586.72[m]$
Distance from RoI2	$D_\Omega = 73.02[m]$	$D_\Omega = 48.02[m]$	$D_\Omega = 57.88[m]$	$D_\Omega = 60.65[m]$
Incident angle	$(\theta_i, \phi_i) = (11.19, 7.27)[deg]$	$(\theta_i, \phi_i) = (28.25, 2.92)[deg]$	$(\theta_i, \phi_i) = (45.51, 178.01)[deg]$	$(\theta_i, \phi_i) = (59.52, 178.30)[deg]$
Reflection angle	$(\theta_r, \phi_r) = (47.07, -165.37)[deg]$	$(\theta_r, \phi_r) = (28.50, -36.10)[deg]$	$(\theta_r, \phi_r) = (15.57, -60.33)[deg]$	$(\theta_r, \phi_r) = (20.65, -39.14)[deg]$
EMS Location	$(x_\Gamma, y_\Gamma, z_\Gamma) = (297, 864, 15)[m]$	$(x_\Gamma, y_\Gamma, z_\Gamma) = (275, 808, 15)[m]$	$(x_\Gamma, y_\Gamma, z_\Gamma) = (279, 754, 15)[m]$	$(x_\Gamma, y_\Gamma, z_\Gamma) = (301, 739)[m]$
Incident field strength	$E_{rms} = 94.3[dB\mu V/m]$	$E_{rms} = 89.76[dB\mu V/m]$	$E_{rms} = 89.95[dB\mu V/m]$	$E_{rms} = 81.31[dB\mu V/m]$
Reflected power	$P_\Gamma = -15.50[dBm]$	$P_\Gamma = -17.80[dBm]$	$P_\Gamma = -20.08[dBm]$	$P_\Gamma = -21.30[dBm]$

Table 3.2: Region of Interest 2 data

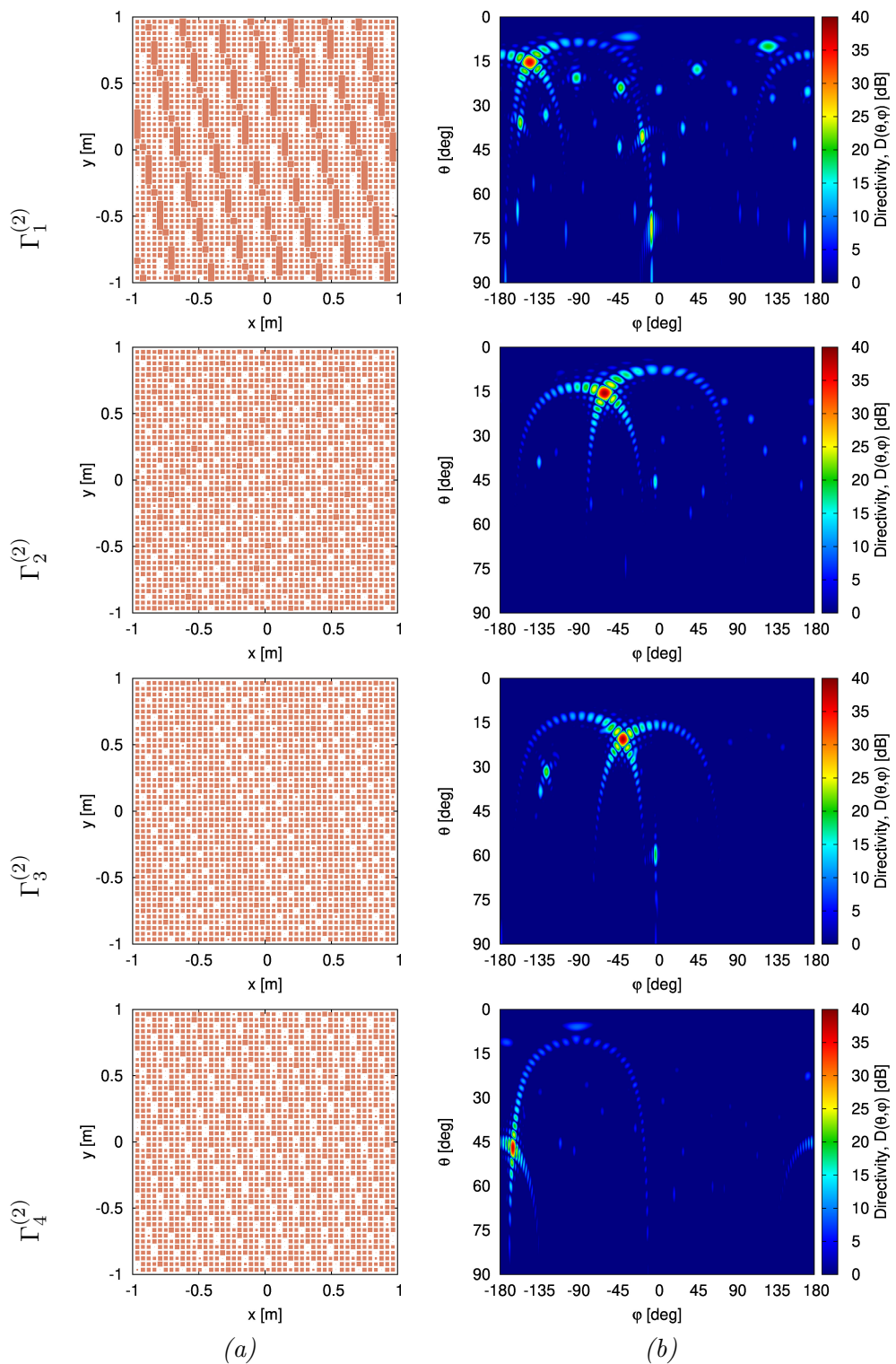


Figure 3.10: (a) Layout - (b) Directivity

Smart Skins Performance

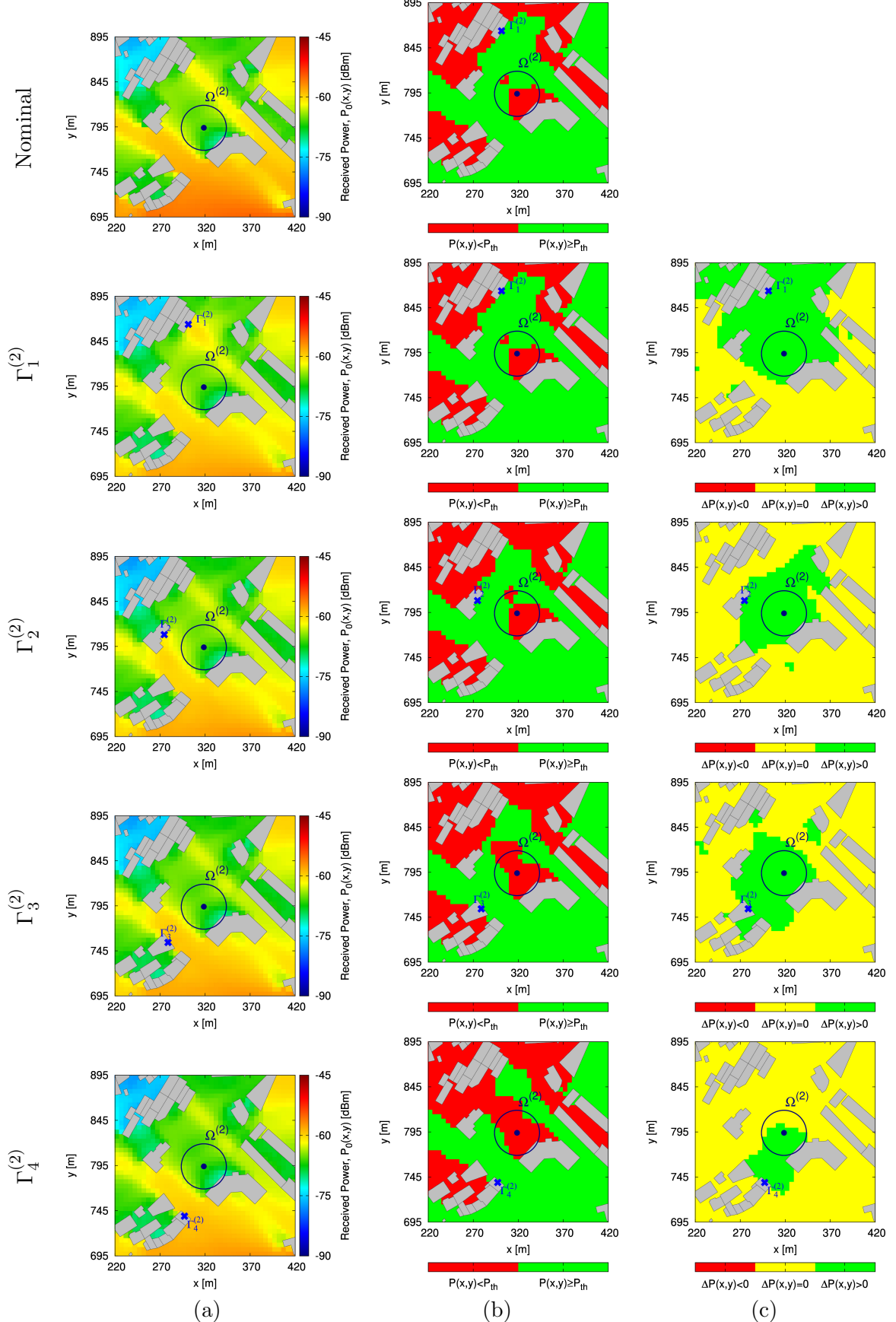


Figure 3.11: (a) Nominal BTS Power Performance vs Smart Skin Performance in Region of Interest 2 - (b) (a) Nominal BTS Thresholded Power Performance vs Thresholded Smart Skin Performance in Region of Interest 2 - (c) Difference between received and reflected power thresholded at $-65[dBm]$

Best Skin and Overall Implementation

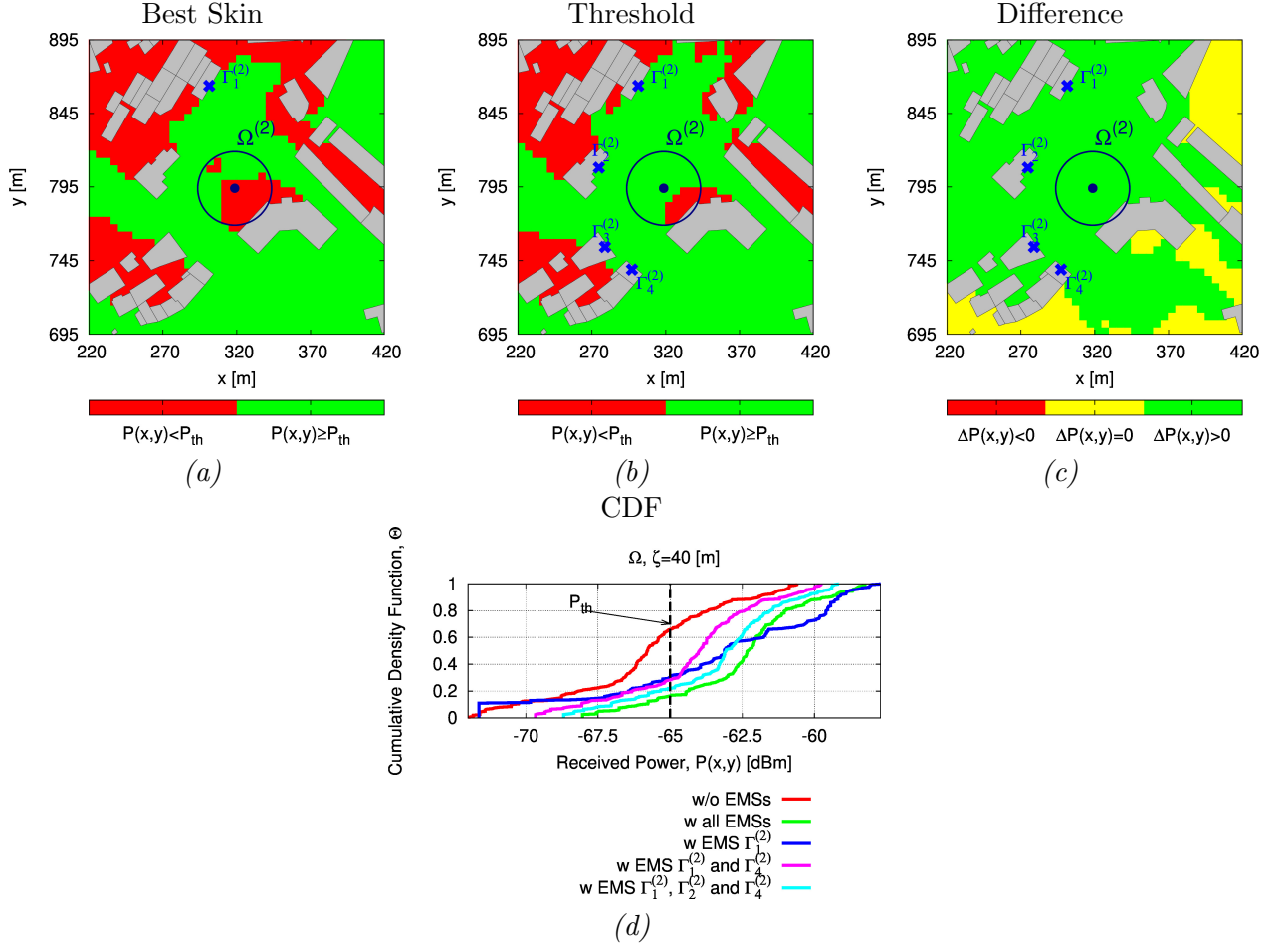


Figure 3.12: (a) - Best Skin for examined Scenario (b) Environment with Smart Skins - (c) Difference between referenced and smart skin implemented Region of Interest - (d) Cumulative Density Function [-65dBm]

3.2.7 Enhancement Region of Interest 3

Smart Skin Sizing and Layout

#	$\Gamma_1^{(3)}$	$\Gamma_2^{(3)}$
Shape	Square	Square
EMS Side	$d = 2[m]$	$d = 2[m]$
Number elements along x	$N_x = 50$	$N_x = 50$
Number elements along y	$N_y = 50$	$N_y = 50$
Distance from BTS	$D_\Psi = 613.80[m]$	$D_\Psi = 615.41[m]$
Distance from RoI3	$D_\Omega = 30.74[m]$	$D_\Omega = 42.90[m]$
Incident angle	$(\theta_i, \phi_i) = (2.87, 150.77)[deg]$	$(\theta_i, \phi_i) = (7.37, 169.05)[deg]$
Reflection angle	$(\theta_r, \phi_r) = (57.67, -148.68)[deg]$	$(\theta_r, \phi_r) = (69.49, -160.37)[deg]$
EMS Location	$(x_\Gamma, y_\Gamma, z_\Gamma) = (1187, 136, 15)[m]$	$(x_\Gamma, y_\Gamma, z_\Gamma) = (1175, 127, 15)[m]$
Incident field strength	$E_{rms} = 88.14[dB\mu V/m]$	$E_{rms} = 94.76[dB\mu V/m]$
Reflected power	$P_\Gamma = -20.51[dBm]$	$P_\Gamma = -20.27[dBm]$

Table 3.3: Region of Interest 3 data

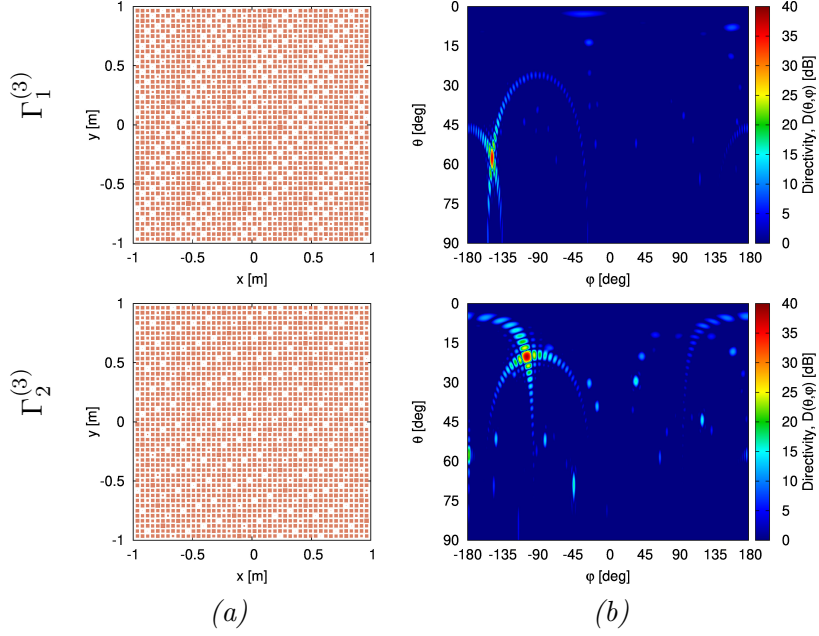


Figure 3.13: (a) Layout - (b) Directivity

Smart Skins Performance

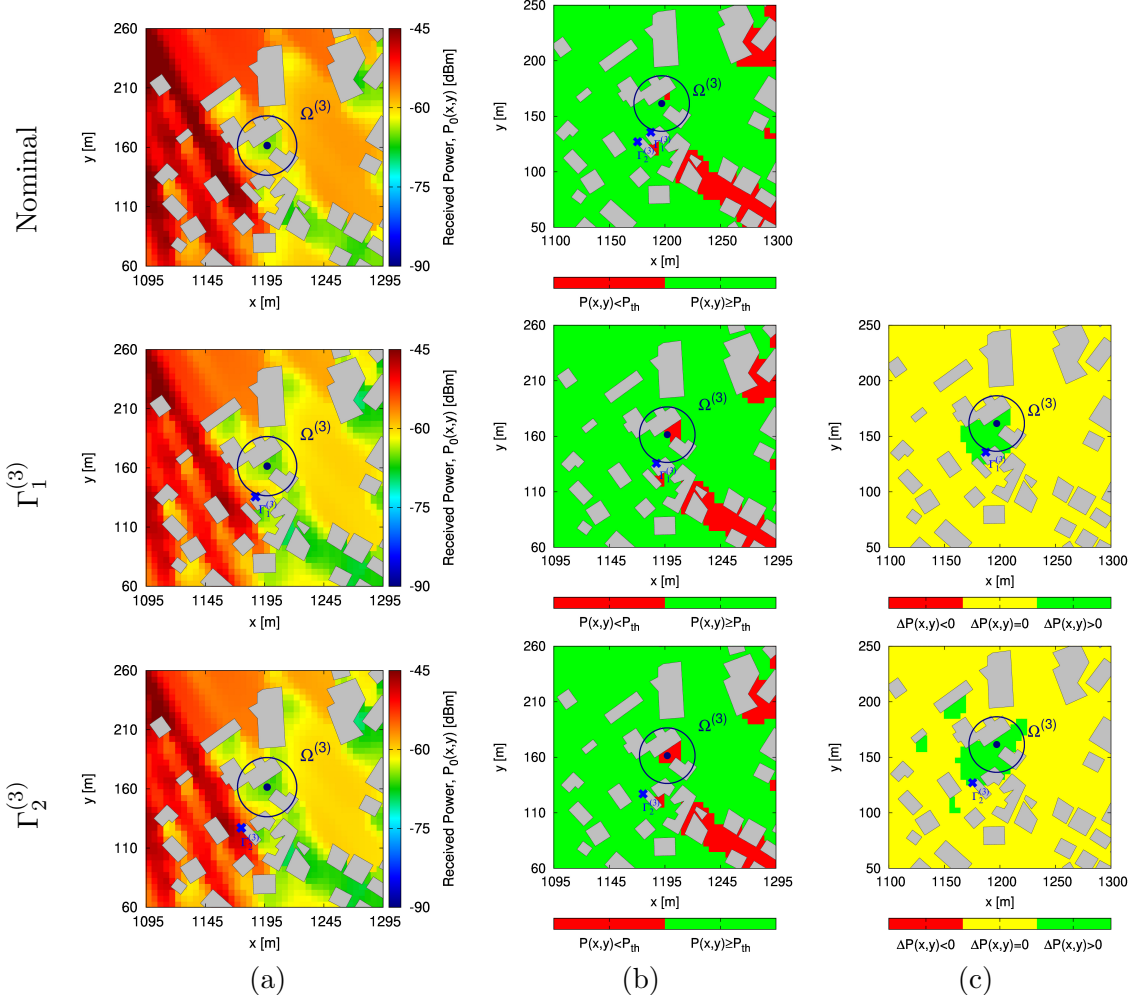


Figure 3.14: (a) Nominal BTS Power Performance vs Smart Skin Performance in Region of Interest 3 - (b) Nominal BTS Thresholded Power Performance vs Thresholded Smart Skin Performance in Region of Interest 3 - (c) Difference between received and reflected power thresholded at $-65[dBm]$

Best Skin and Overall Implementation

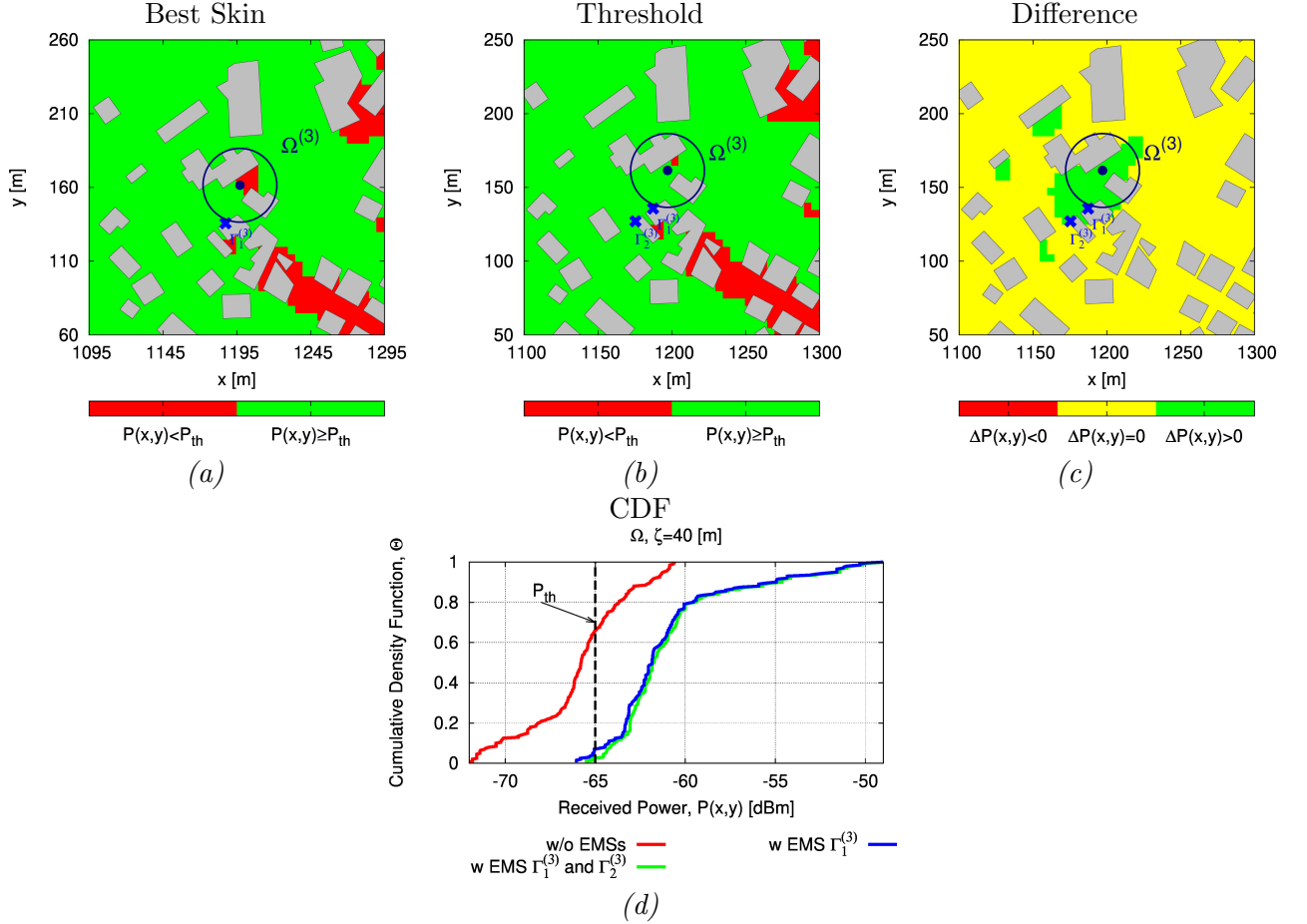


Figure 3.15: (a) - Best Skin for examined Scenario (b) Environment with Smart Skins - (c) Difference between referenced and smart skin implemented Region of Interest - (d) Cumulative Density Function [-65dBm]

Chapter 4

Conclusions

As for the conclusions, it is going to be first examined the State-of-Art analysis and secondly the Planning EM work.

4.1 State-of-Art Conclusions

As discussed in the previous sections, the addressed possibility to efficiently and effectively synthesize inexpensive smart EM skins supporting advanced beamforming capabilities is possible. More specifically, the design of passive/static smart skins with enhanced wave manipulation capabilities has been formulated within the *GSTC* theoretical framework by exploiting an *IS* formulation. The *IPT* design and *SbD* optimization process has been largely discussed, since these two methods were the founding

for the experimentation carried through this paper.

As can be clearly seen, the use for *SPSS* is justified since the performance fulfilled the expectations and the design was rather straightforward.

In the final part of the 2.1.2, has been stated that even a complex footprint can be handled. Observations will now follow:

1. with the exception to the smallest apertures (i.e. $P \times Q = 25 \times 25$), the proposed *IPT-SbD* approach can handle complex footprints, as seen in the Cost Function Diagram (Fig.2.11);
2. as expected, it profitably leverages the increased number of descriptors of wider apertures to improve the beamforming accuracy as quantitatively confirmed by the behavior of $\mathcal{X}^{SPSS} = \mathcal{X}^{SbD}$ and \mathcal{X}^{IPT} in Fig.2.11 and Table 2.1 as well as by the evolution of the *IPT* process versus the iteration number h ($h = 1, \dots, H$) [Fig.2.11(b)];
3. the *surface current fidelity index* is not significantly affected by the aperture size, as can be seen from Fig.2.11(c);
4. the entire synthesis process turns out to be extremely efficient whatever the number of *DoFs* and pattern footprint.

As a representative example, picking the most complex footprint in the study case ($P \times Q = 400 \times 400$), the whole *CPU* time is $\Delta t^{IPT} + \Delta t^{SbD} \approx 1066.1[s] \simeq 18[min]$, which significantly lower than $\Delta t^{PSO} \approx 115[days]$

The effectiveness of the *IPT-SbD* method has been proved.

But, as stated in 1, one of the key aspects that a smart skin needs to have, caused by its place of application, which is a urban environment, is its aesthetic design: as formulated the material of the smart skin needs to be as thin as possible to not compromise the outline of the building. With the previous formulation, it's been stated that the smart skin material is a combination of reflective and dielectric material, combined in sheets; since the need to design an inexpensive is absolute for the sake of the formulation, is intended that there is no excess use for the material, which follows the need to not waste any material, for example, when increasing the thickness. This statement proves again the effectiveness of the formulation and the design, since the aim was to create a mask as simple and inexpensive as possible.

In conclusion, it's been stated that the numerical and experimental results confirms the effectiveness of the proposed design process for constructing simple yet high-performance metasurfaces that can efficiently handle large apertures. Future applications of the proposed design process, other than the ones descriptive in [8], can be the replacing of the current urban outline: since the experimentation with two different complex masks, which resembled the logo for the "IEEE" organization and the "ELEDIA" Research Center, a possible future application for this design could be to replace the existing company logo signs with a "Smart" sign made by inexpensive yet high-performance reflective material, which can improve the wireless coverage, and all other already-stated requirements, without the need to be replaced or to receive maintenance.

4.2 Planning EM Conclusions

Each RoI has been choosed to see how well the EMS, or EMSs, could have improved the SEE. The first RoI was the "middle ground", a region not too weak, but with enough requirements to at least been chosen. The second RoI was the worst of it all, since the region was quite wide and the reflected power was almost on the lower limit for the received power. The third one was the "best" region, since it's received power was quite a lot. Having these three kinds of RoI was helpful to analyze and improve various scenarios, emphasizing the versatility of the EMS.

As for the results, the CDF values are going to be listed to show the improvement:

- RoI 1: Before improvement: ca. 33% - After improvement: ca. 17%
- RoI 2: Before improvement: ca. 65% - After improvement: ca. 19%

- RoI 1: Before improvement: ca. 63% - After improvement: ca. 5%

In conclusion, it can be stated that EMSs are useful to improve weak areas inside the coverage region on the BTS. Some issues to consider are the cost of the EMSs, the difficulty of obtaining information for the RoI, the BTS and the Applications spots. Other than that, the discussed formulation has been successful, having improved all of the considered RoIs.

4.3 Final conclusions

In this discourse, a wide range of telecommunication improvements has been shown: as documented in the State-of-Art Analysis, various EMSs have been proposed, deeply analyzing how the shape and its configuration affects the performance of said EMS. In [8], has been clearly stated the effectiveness of EMSs in a urban environment and the creation of a RIS-based wireless communication is the way to follow to reach an improvement when a building crowded area hinders the possibility for the user to have a good quality service. From an economical point-of-view, the installation of multiple EMSs is much more reasonable than raising the power consumption of a BTS. And since the ISP can't pretend that the user changes its device just for improving the connectivity, a RIS-aided environment is clearly the best option. It has been clearly shown that RISs are great power handlers and its ability to be reconfigured make them easily applicable in all kinds of environments. But since they are an innovative technology, they are not vastly employed. For the ISPs, to improve all of their weak regions in all of their covered towns, its a large investment. But in these recent years, the development of RISs has come a great way, as shown from the papers aforementioned. From formulations to real-life test cases, this technology is developing at a really fast rate, and that brings the last point of this section. Thanks to the great work of other researchers, RISs will become a needed resource when planning a EM environment, especially in urban areas, where EM and physical obstructions are a problem that needs to be taken into account. The potential that RISs have is vast, so the case studies for their employment is not limited. In simple terms, it can be said that, from SPSSs to RISs, an improvement in performance, computational times and energy consumption is clear. So the employment of these technology is greatly incentivized in EM disturbed environments, where the BS is too far away and planting another BS is unnecessary or where there is the need to improve the coverage.

Bibliography

- [1] A. Benoni, M. Salucci, G. Oliveri, P. Rocca, B. Li, and A. Massa. Planning of em skins for improved quality-of-service in urban areas,. *arXiv*, 2021.
- [2] F. Costa and M. Borgese. Electromagnetic model of reflective intelligent surfaces. *IEEE O. J. Commun. Soc.*, 2:1577–1589, 2021.
- [3] L. Dai et al. Reconfigurable intelligent surface-based wireless communications: Antenna design, prototyping, and experimental results. *IEEE Access*, 8:45913–49923, 2020.
- [4] P. Rocca et al. On the design of modular reflecting em skins for enhanced urban wireless coverage. *IEEE Trans. Antennas Propag.*, 2022.
- [5] X. Pei et al. Ris-aidedwireless communications: Prototyping,adaptive beamforming, and indoor/outdoorfield trials. *IEEE Trans. Commun.*, 69(12):8627–8640, 2021.
- [6] H. Gacanin and M. Di Renzo. Wireless 2.0: Toward an intelligent radio environment empowered by reconfigurable meta-surfaces and artificial intelligence. *IEEE Veh. Technol. Mag.*, 15(4):74–82, 2020.
- [7] Q. Liu, S. Sun, B. Rong, and M. Kadoch. Intelligent reflective surface based 6g communications for sustainable energy infrastructure. *IEEE Wireless Commun.*, 28(6):8627–8640, 2021.
- [8] G. Oliveri, P. Rocca, M. Salucci, and A.Massa. Holographic smart em skins for advanced beam power shaping in next generation wireless environments. *IEEE J. Multiscale Multiphys. Comput. Tech.*, 6:171–182, 2021.
- [9] G. Oliveri, F. Zardi, P. Rocca, M. Salucci, and A.Massa. Building a smart emenvironment-ai-enhanced aperiodic micro-scale design of passive em skins. *IEEE Trans. Antennas Propag.*, 2022.
- [10] C. You and R. Zhang. Wireless communication aided by intelligent reflecting surface: Active or passive? *IEEE Wireless Commun. Lett.*, 10(12):2659–2663, 2021.
- [11] H. Zhang, B. Di, Z. Han, H. V. Poor, and L. Song. Reconfigurable intelligent surface assisted multi-user communications: How many reflective elements do we need? *IEEE Wireless Commun. Lett.*, 10(5):1098–1102, 2021.